JOURNAL OF Materials Feature Article CHEMISTRY

A novel property caused by frustration between ferroelectricity and antiferroelectricity and its application to liquid crystal displays—frustoelectricity and V-shaped switching

Takahiro Matsumoto,[a,b] Atsuo Fukuda,*[a] Masahiro Johno,[b] Yuki Motoyama,[b] Tomoyuki Yui,[b] San-Seong Seomun[c] and Mamoru Yamashita[d]

[a]*Department of Kansei Engineering, Faculty of Textile Science and Technology, Shinshu University, Ueda-shi, Nagano-ken 386–8567, Japan*
[b]*Info-Advanced Materials Department, Tokyo Factory, Mitsubishi Gas Chemical Company, Inc., 1–1, Niijuku 6-chome, Katsushika-ku, Tokyo 125–8601, Japan*
[c]*Department of Polymer Chemistry, National Institute of Materials and Chemical Research, Tsukuba-shi, Ibaraki-ken 305–8565, Japan*
[d]*Department of Physics Engineering, Faculty of Engineering, Mie University, Tsu-shi, Mie-ken 514–8507, Japan*

Received 26th April 1999, Accepted 8th June 1999

We have studied the frustration between ferro- and antiferro-electricity in chiral smectic C like liquid crystalline phases, which is not only fundamentally interesting but also very attractive from an application point of view. It causes temperature induced successive phase transitions as characterized by a devil's staircase and the thresholdless, hysteresis-free, V-shaped switching induced by an applied electric field. The devil's staircase indicates some type of interlayer ordering, while the V-shaped switching suggests considerably diminished tilting correlation. These two are apparently contradictory to each other, but result from the same cause, *i.e.* the frustration. We have first summarized experimental facts regarding subphases and successive phase transitions observed in many compounds and mixtures, which we believe are related to one another and result from the frustration. We have introduced several different theoretical explanations for these observed facts, and shown that only the axial next nearest neighbor Ising (ANNNI) model can explain almost all of the facts, provided that it is unified with the XY model appropriately. The unified model can make a comprehensive explanation in the most natural way based on the most probable molecular interactions. We have then emphasised that there are several modes regarding the V-shaped switching, because the system becomes so soft with respect to the tilting direction and sense that any additional external or internal force modifies the in-plane local director alignments. For the practically usable ones, we have emphasised the need for some type of randomization in the molecular alignment at the tip of the V and/or the switching process. In particular, the two dimensional (ideally, cylindrically symmetric) azimuthal angle distribution of local in-plane directors around the smectic layer normal is most attractive. Such a randomized state at the tip of the V is thermodynamically unique under a given condition imposed by interfaces. It stays stable even when the smectic layer structure, such as a chevron, changes with temperature. Finally, we have summarized the so-far reported compounds and mixtures for the V-shaped switching and introduced some prototypes of LCDs using them.

1. Introduction

Before the discovery of the antiferroelectric chiral smectic C_A phase (SC_A*) in MHPOBC, compound **1** in Table 1,[1] it was considered that the packing entropy effect together with the Maier–Saupe type intermolecular interaction causes the tilting in the same direction and sense,[2,3] aside from a slight precession from layer to layer due to chirality and flexoelectricity; the ferroelectric chiral smectic C* phase (SC*) as well as the achiral smectic C phase (SC) was the only tilted fluid smectic phase. The discovery showed that the interlayer antiferroelectric ordering can be stabilized in a mesophase without long-range positional order. This was a surprising and fundamental condensed matter finding[4] and prompted intensive research into the structure and properties of SC_A*. Intensive research has disclosed several unexpected aspects of frustration between ferro- and antiferro-electricity.[5] The frustration is not only fundamentally interesting but also very attractive from an application point of view. It causes temperature induced successive phase transitions as characterized by a devil's staircase[6] and the thresholdless, hysteresis-free, V-shaped switching induced by an applied electric field.[7–9] The devil's staircase indicates some type of interlayer ordering, while the V-shaped switching suggests considerably diminished tilting correlation. These two are apparently contradictory to each other, but result from the same cause, *i.e.* the frustration mentioned above.

We would not expect to encounter the devil's staircase in liquid crystals, because it seems easy to lift any degeneracy by continuously changing the molecular orientations in some way.[10] In fact, the SC*- and SC-like phases have two degrees of freedom, the polar angle θ and azimuthal angle φ. An infinite number of interlayer orderings can be constructed by modulating φ from layer to layer. Changes among them, however, seem to be continuous and may not occur as phase transitions. Modulating θ from layer to layer is not realistic, because it changes the smectic layer thickness and costs too much distortion energy. The anticlinic structure ($\varphi = 0$ and π) of SC_A* may be stabilized by strong orientational correlations between the transverse dipoles of neighboring molecules in adjacent layers, which result in a short range interaction.[11] Consequently, the axial next-nearest neighbor Ising (ANNNI) model can be a candidate for the devil's staircase mentioned above by assigning the tilting senses,[12] right and left, in a smectic layer to the ± 1 Ising spins. One of the two purposes of this Feature Article is to clarify the applicability and limitations of the ANNNI model. The ANNNI model well describes the system under consideration, at least near the ground state, but large azimuthal angle fluctuations come to play an important role near the second order critical curve

above which the disordered phase emerges. The unification of the ANNNI model with the XY model is necessary.[13,14]

The other purpose of this Article is to show that the V-shaped switching can also be understood by that unification. Usually, the transition between SC_A* and SC* is first order; in homogeneous cells, the corresponding electric-field-induced change in optical light transmission shows tristable switching, which is characterized by DC threshold, hysteresis, and domain boundary movement.[15] In some of the compounds and mixtures that exhibit ferro-, ferri-, and/or antiferro-electric phases in free-standing films, however, the V-shaped switching is observed in homogeneous cells; it shows neither threshold nor hysteresis, and occurs quite uniformly with no boundary movement.[7,8,16,17] In such materials, the system is close to the second order critical curve above which the disordered phase emerges, and becomes extremely soft with respect to the tilting direction and sense because of the reduced tilting correlation in a single layer as well as between neighboring layers. Consequently, interface effects may easily disturb the interlayer ordering characteristic of the ordered phase in the bulk, producing some type of randomization in the local in-plane director alignment at the tip of the V and/or in the switching process.[17,18] The V-shaped switching has attracted considerable attention because of a strong demand for liquid crystal displays (LCDs) with active matrix (AM) (thin film transistor (TFT)) electrodes having fast response, wide viewing angle, and high contrast ratio.[19,20]

This article consists of six sections. In Section 2, we explain an important role played by strong orientational correlations between the transverse dipoles of neighboring molecules in adjacent layers in stabilizing anticlinic SC_A and SC_A*. Since this is a rather short range interaction, it may allow the coexistence of synclinic and anticlinic orderings between smectic neighboring layers in a single phase, producing various kinds of ferri- and antiferro-electric phases. Section 3 summarizes experimental facts regarding subphases and successive phase transitions observed in many compounds and mixtures, which we believe are related to one another and result from frustration between ferro- and antiferro-electricity. Section 4 first introduces several different theoretical explanations for these observed facts, and then shows that only the ANNNI model can explain almost all of the facts, provided that it is unified with the XY model appropriately. The unified model can provide a comprehensive explanation in the most natural way based on the most probable molecular interactions. Section 5 is for the V-shaped switching. We emphasise that there are several modes regarding the V-shaped switching, because the system becomes so soft with respect to the tilting direction and sense that any additional external or internal force modifies the in-plane local director alignments. Then, we suggest the practically usable mode. Section 6 summarizes the so-far reported compounds and mixtures for V-shaped switching and introduces some prototypes of LCDs using them.

2. Antiferroelectric liquid crystals

Historical backgrounds concerning the discovery of antiferroelectric liquid crystals (AFLCs) were described in a Feature Article and a review paper published previously.[21,22] The phase structure and the origin of antiferroelectricity were also explained in the Feature Article. Since then, however, remarkable progress has been made and the explanations at that time become insufficient and even inappropriate in some cases. Four important points are: (1) The chiral chain is bent with respect to the rigid core in liquid crystal phases. (2) In-plane spontaneous polarizations mainly exist near smectic layer boundaries parallel to the tilt plane in antiferroelectric SC_A* and perpendicular to it in ferroelectric SC*. (3) During the pretransitional phenomenon, which is very conspicuous in some electric-field-induced phase transitions from SC_A* to SC*, molecular tilting directions in adjacent layers are not coplanar, *i.e.* neither synclinic ($\varphi=0$) nor anticlinic ($\varphi=0$ or π); it is considered that tilting directions in adjacent layers are correlated with the biased directions of molecular rotations about the long axes. (4) The instant (nonaveraged) dipole–dipole interaction, *i.e.* orientational correlations between the transverse dipoles of neighboring molecules in adjacent layers, can stabilize the anticlinic SC_A* as well as SC_A structure, although the averaged dipole–dipole interaction between all the molecules vanishes.

The bent molecular shape has been confirmed in SA, SC*, SC_A*, SI* and SI_A* by X-ray diffraction,[23] polarized IR spectroscopy,[24,25] ^{13}C-NMR,[26] ^{2}H-NMR[27] and a chemical method.[28,29] Fig. 1 shows the herringbone molecular arrangement in a crystal structure of compound **2** in Table 1 reported by Okuyama *et al.*,[30] which allows us to imagine the arrangement in SC_A*. In liquid crystalline phases, molecules are exposed to thermal agitations that excite various internal and as-a-whole molecular motions. In particular, molecules are rotating around their long axes and the center of mass distribution along the layer normal is gaussian. It is useful to visualize the components of polarization (dipole moment density) averaged over the X and Y directions, $p_X(Z)$ and $p_Y(Z)$. Conventionally, the liquid crystal coordinate system is chosen in such a way that the Z axis is parallel to the smectic layer normal and the X axis is in the tilt plane. Although detailed calculations have not yet been performed, Fig. 1 clearly indicates that both $|p_X(Z)|$ and $|(p_Y(Z)|$ have large values near the boundary and become almost zero near the center of smectic layers. Note that large transverse dipole moments exist near the chiral center. Symmetry requires that the in-plane spontaneous polarizations at boundaries should be parallel to the tilt plane in SC_A* and perpendicular to it in SC*. Consequently, in tristable switching, changes in molecular arrangements and in-plane spontaneous polarizations are more appropriately described as illustrated in Fig. 2.[30–34]

In a homogeneous cell placed between crossed polarizers, whose axes are parallel and perpendicular to the smectic layer normal, an increase in the transmittance is observed even

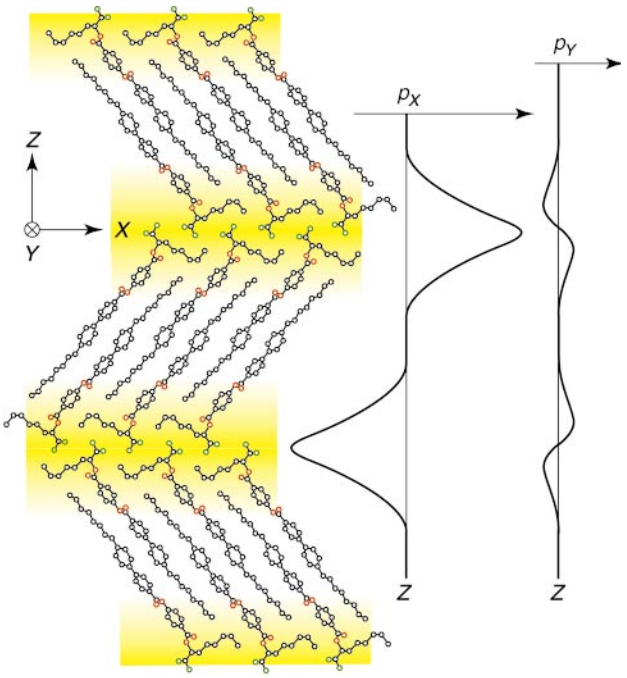

Fig. 1 Illustrations of the anticlinic, herringbone molecular arrangement[30] in a crystal structure of compound **2** in Table 1. The components of polarization (dipole moment density) averaged over the X and Y directions, $p_X(Z)$ and $p_Y(Z)$, are predicted and also drawn schematically in liquid crystalline SC_A*.

Table 1 List of compounds cited in the text. Compounds **1** and **3** are prototype antiferroelectric liquid crystals. The Mitsui mixture of **9:10** = 63:37 and the Inui mixture of **11:12:13** = 20:40:40 are for V-shaped switching

1	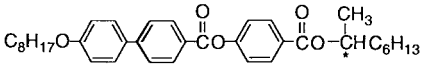
2	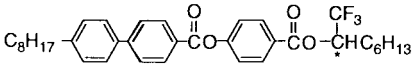
3	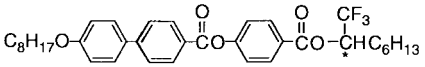
4	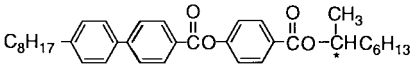
5	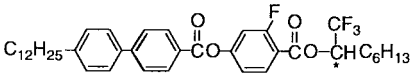
6	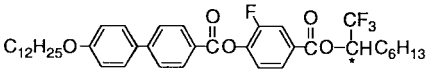
7	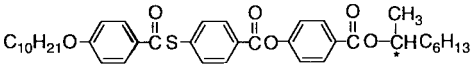
8	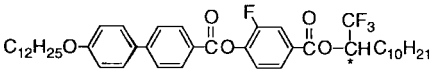
9	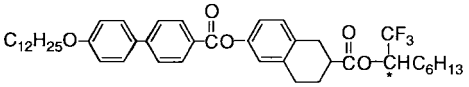
10	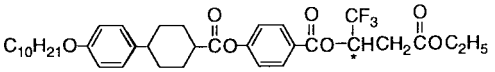
11	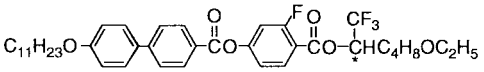
12	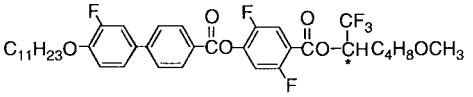
13	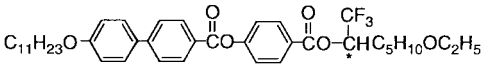
14	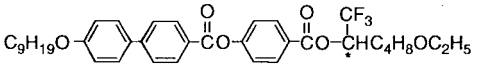
15	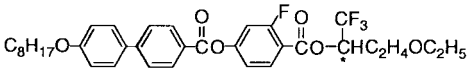
16	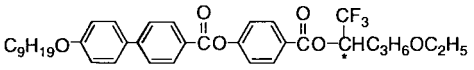

below the threshold field. This is a pretransitional phenomenon, which may be conspicuous in some materials but not in others as given in Fig. 5 of Ref. 35. Let us consider what is happening in the tilt directions and the rotational states of molecules around their long axes.[35] Fig. 3 illustrates a thought experiment. An electric field is applied parallel to the page. A low enough field can unwind the helicoidal structure of SC_A^* and the tilt plane becomes parallel to the field due to the dielectric anisotropy of SC_A^*. In-plane spontaneous polarizations emerge at boundaries parallel to the X axis. An electric field higher than the threshold induces SC*. The conventional liquid crystal frame rotates by 90 degrees. The tilt plane (the ZX plane) now becomes perpendicular to the field (the Y axis) and in-plane spontaneous polarizations located at boundaries are parallel to the Y axis on the page. Even in the pretransitional process, the field and hence in-plane spontaneous polarizations at boundaries are always parallel to the

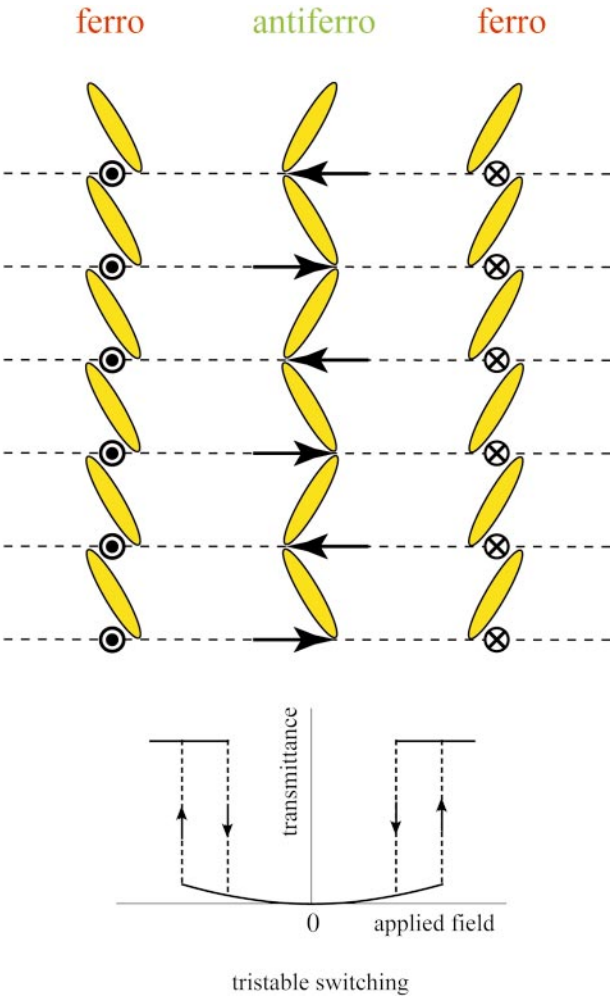

Fig. 2 Molecular arrangements and in-plane spontaneous polarizations in the tristable switching.

page. The tilt directions are neither parallel nor perpendicular to the page. The directions are conveniently specified by the projections of the molecular long axes onto a boundary as shown in the upper and lower part of Fig. 3; thin solid and dotted lines in circles indicate the projections. In a boundary with $+P_X$, the in-plane spontaneous polarization changes into $+P_Y$ without becoming zero (without changing its polarity). In another boundary with $-P_X$, it may become zero because its polarity is just opposite. Fig. 3 was drawn for *S*-MHPOBC, where the C=O moiety near the chiral center mainly produces positive spontaneous polarization in SC*.

Let us consider the rotational states of molecules around their long axes. The molecular frame is defined as given in the lower part of Fig. 3; there are four equivalent molecular states because of the SC* and SC_A^* symmetry. The biased direction is specified by the rotational angle around the z axis, ψ, where the positive value represents the rotation of a right-handed screw moving along the z axis in the positive sense and $\psi = 0$ is the x axis. Near the chiral center, the two moieties, C=O and CF_3, have large transverse dipole moments in TFMHPOBC, compound **3**, while only the C=O moiety has a large transverse dipole moment in MHPOBC, compound **1**. Their rotational distribution around the molecular long axis (the eigen axis of the smallest moment of inertia) affects $P_X(Z)$ and $P_Y(Z)$ most seriously. The distribution of C=O in *S*-MHPOBC has been studied in detail by polarized IR spectroscopy. It is cylindrically symmetric in SA but is biased in SC* and SC_A^*. The biased directions are ${\psi_0}^F \sim -75 \sim -85^\circ$ in SC* and ${\psi_0}^{AF} \sim -45 \sim 45^\circ$ in SC_A^*, respectively. The point is that ${\psi_0}^F$ and ${\psi_0}^{AF}$ are different. The in-plane spontaneous

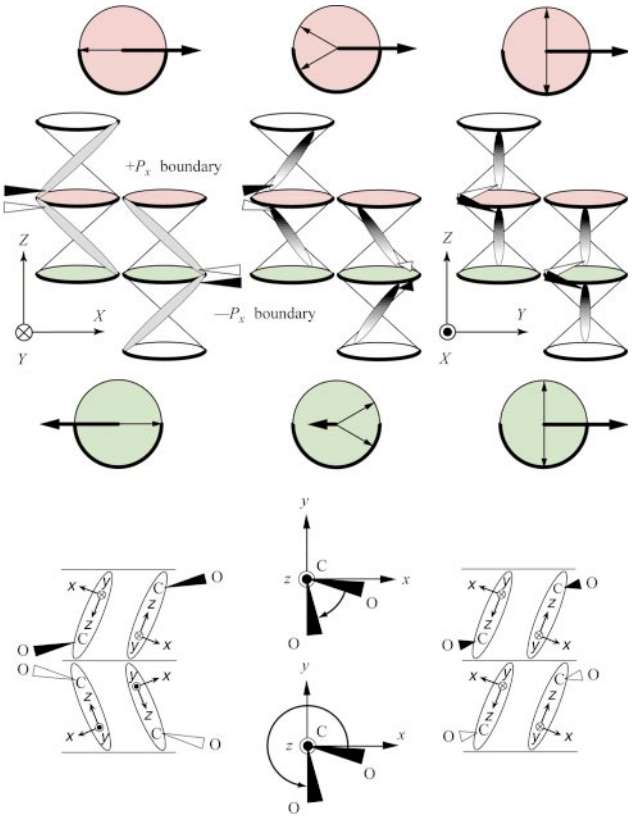

Fig. 3 Schematic illustrations of the tilt directions and the rotational states of molecules around their long axes during a pretransitional process of the tristable switching.[35]

polarizations at boundaries should be parallel and perpendicular to the tilt plane; but the biased directions may not be exactly parallel or perpendicular because of the two-fold symmetry around the X and Y axes. During the pretransitional process, $\psi_0{}^{AF}$ rotates toward $\psi_0{}^{F}$ clockwise in the $+P_X$ boundary and counterclockwise in the $-P_X$ boundary, respectively. The tilting directions in adjacent layers are correlated with the biased directions of molecular rotation about the long axis. More generally, we can say that the molecular rotation about their long axes strongly couples with their azimuthal angle rotation about the smectic layer normal. Symmetry requires that the in-plane spontaneous polarization on a boundary is parallel to the bisector of the projected directions in the upper and lower layers and that its magnitude depends on the C-directors. It is quite natural to speculate that this relation holds generally between the in-plane spontaneous polarization on a boundary and the tilt directions and senses of molecules in the upper and lower layers.

If we neglect the slight precession of at most a few degrees per layer caused by chirality, the molecular tilting directions (specified by the azimuthal angle φ) are considered coplanar not only in ferroelectric SC* ($\varphi=0$) but also in antiferroelectric SC_A* ($\varphi=0$ or π). Recently, Mach *et al.*[4] were successful in observing directly the double-layered periodicity by resonant X-ray scattering. They confirmed that in-plane directors in adjacent layers are exactly parallel to a plane in SC_A and almost exactly in SC_A*, detecting the small splitting of half-order diffracted peaks in SC_A* due to the chirality induced helicoidal structure. It has been well established that SC_A and SC_A* have the anticlinic herringbone structure. There should exist the intermolecular interaction that stabilizes the anticlinic SC_A and SC_A* structure. A number of microscopic origins for the interaction have been proposed.[21,31,36,37] Considering the thermally activated molecular rotation around the long axes, however, we could not conclude that they explained explicitly why and how the anticlinic structure in SC_A and SC_A* is

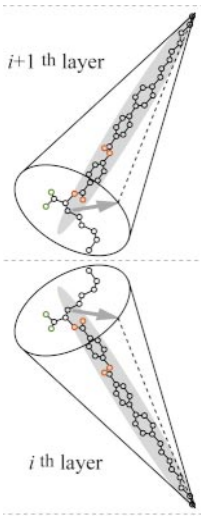

Fig. 4 A schematic illustration of strong dipole–dipole correlations between neighboring molecules in adjacent layers that stabilize the anticlinic SC_A and SC_A* structure.

stabilized. Quite recently, Osipov and Fukuda[11] determined the mathematical form of the interaction that promotes the anticlinic SC_A and SC_A* structure, showing that it is stabilized by some specific intermolecular interaction; conventional dispersion interactions between typical mesogenic molecules do not stabilize the anticlinic SC_A and SC_A* structure as against the synclinic SC and SC* structure. There exist strong dipole–dipole correlations between neighboring molecules in adjacent layers and these correlations are responsible for the stabilization as illustrated in Fig. 4. Since this is a rather short range interaction, it may allow the coexistence of synclinic and anticlinic orderings between smectic neighboring layers in a single phase, producing various kinds of ferri- and antiferroelectric phases.

3. Subphases and successive phase transitions—devil's staircase

3.1. Historical backgrounds and a possible most general subphase sequence

At the outset of disclosing antiferroelectric SC_A* in compound **1**, MHPOBC, three other SC*-like phases were observed. Chandani *et al.*[38] designated these phases as SC_α*, SC_β* and SC_γ* in order of decreasing temperature, identifying SC_β* as ordinary ferroelectric SC*.† By analyzing the electric field dependence of the conoscopic figure and of the apparent tilt angle, Gorecka *et al.*[44] soon proved that SC_γ* is a ferrielectric phase. Two years later, Okabe *et al.*[45] found another antiferroelectric phase designated as AF in compound **4**. Stimulated by this finding, Isozaki *et al.*[6,46,47] made systematic investigations on the electric field–temperature (E–T) phase diagram in several compounds and mixtures. They confirmed that at least three ferrielectric and one antiferroelectric subphase may emerge between SC_A* and SC*, suggesting that these subphases constitute a part of a devil's staircase formed by frustration between ferro- and antiferro-electricity in liquid crystals. Their suggestion was further supported by the emergence of an additional ferrielectric phase designated as FI on the high temperature side of AF in compounds **5** and **6**.[48,49] In this way, Itoh *et al.*[50] presented in 1997 a possible, most general phase sequence given in Fig. 5.

†When the enantiomeric excess is high, SC_β* is different from SC* and may belong to spr1 or 2.[39–42] Gleeson *et al.*[43] treated SC_β* in a way completely different from ours. Our standpoint is that all the subphases under consideration result from a common cause; on the other hand, they tried to explain SC_β* alone separately.

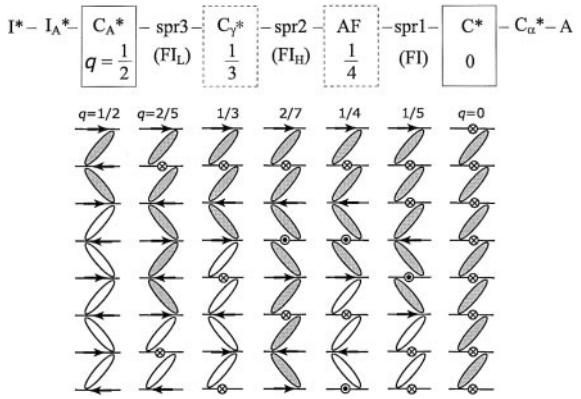

Fig. 5 A possible most general subphase sequence.[50]

Some of the phases may not actually occur in a particular compound or mixture but, when they do exist, they follow this order. A few additional subphases seem to emerge in the vicinity of FI_L and FI_H.[47] Likewise, some subphases other than FI are expected in the temperature region between AF and SC*. Consequently, we designated these regions as spr1, spr2, and spr3, respectively, where spr refers to subphase region. SC_α* is an SC*-like phase and may emerge just below SA.‡ It is closely related to other subphases between SC_A* and SC* but does not belong to the devil's staircase. SI* and SI_A* are hexatic versions of fluid SC* and SC_A*, and do not belong to the devil's staircase either. Interestingly, SI_A* is the higher temperature phase of SI*.[52] Since both SC* and SI* have the same symmetry, SC* may change into SI* continuously.[53–55]

Calorimetric studies[56–59] have been performed in several compounds, clarifying the following two facts: (1) the subphases between SC_A* and SC* are clearly discriminated by the first order phase transitions; and (2) the enthalpies and entropies gained at the respective phase transitions are extremely small. Quite recently, Mach *et al.*[4] reported the first direct structural observation of distinct multilayer periodicities by resonant X-ray scattering. They confirmed the three-layer ($q=1/3$) and four-layer ($q=1/4$) periodicities in what they called ferri 1 and ferri 2 phases, respectively, in compound **7**. Nguyen *et al.*[55] identified the ferri 1 phase as SC_γ* by a miscibility test. Since our various experiences lead us to believe that the ferri 2 phase must be antiferroelectric and miscible with AF, we studied the electric-field-induced change of the conoscopic figure and confirmed its antiferroelectric character by using the compound supplied by Nguyen.[59] As exemplified above, conoscopic observation under an applied electric field has been used in identifying the ferro-, ferri-, or antiferro-electric character of a particular phase. The characteristic conoscopic figures under an applied electric field are shown in Fig. 6, where the corresponding indicatrix ellipsoids of refraction and the molecular arrangements based on the Ising model are also given. These figures are the same as those illustrated in the previous Feature Article.[21] However, the in-plane spontaneous polarizations are now considered to exist at smectic layer boundaries, represented by arrows parallel and perpendicular to the tilt plane. They were located in the middle of smectic layers and hence represented arrows perpendicular to the tilt plane alone. The polarization $\boldsymbol{p}(Z)$ is considerably localized as schematically illustrated in Fig. 1. This localization resolves the issue raised in a textbook about the term ferrielectricity and the unlikely (improbable) partial compensation of the spontaneous polarizations.[60]

‡In the previous Feature Article,[21] frustration between ferro- and antiferro-electricity was considered to form another devil's staircase in SC_α*. Yamada *et al.*[51] showed, however, that SC_α* emerges even when the spontaneous polarization is zero and the helicoidal pitch becomes infinite.

3.2. Characteristic electric field dependence of apparent tilt angles and conoscopic figures

Let us summarize the electro-optical properties of these subphases. Fig. 7 shows the apparent tilt angle as a function of an applied electric field in compound **1**.[61] The plateau due to SC_γ* exists stably and has nearly the same apparent tilt angle, which is about 1/3 of the saturated value in SC*. Likewise, the spontaneous polarization in SC_γ* is about 1/3 of that in SC*. Because of the 1/3 character of the apparent tilt angle as well as the spontaneous polarization, Gorecka *et al.*[44] identified SC_γ* as ferrielectric and Takezoe *et al.*[62] proposed the Ising model as given in Fig. 5 and 6. The Ising model can also explain the electric field dependence of the conoscopic figures naturally. Let us consider the indicatrix ellipsoid in SC_γ* with the right handed X', Y' and Z' principal axes. The Z' axis is in the tilt plane and tilts from the smectic layer normal by about 1/3 of the molecular tilt angle, and the Y' axis is perpendicular to the tilt plane. The molecular tilt angle is less than 45° and the molecules are most easily polarizable along the molecular long axis. Consequently, the Z' axis has the largest refractive index and the Y' axis has the smallest one. Because of the remaining ferrielectric in-plane spontaneous polarizations, the helicoidal structure of SC_γ* is completely unwound in the plateau region and the tilt plane becomes perpendicular to an applied electric field (the Y' axis). The direction connecting melatopes should be in a plane containing the viewing direction (the smectic layer normal in the present case) and the axis with the smallest refractive index; hence the melatopes appear parallel to the electric field.

It is worthwhile noticing that at least three subphases, FI_L, FI_H and FI in the spr3, 2 and 1 regions are confirmed to exist without applying any electric field,[50] as illustrated in Fig. 8(a). These subphases show the characteristic electric field dependence of the conoscopic figures similar to that of SC_γ*, *i.e.* the melatopes appearing parallel to the electric field.[44–50] Two examples in FI_L ($q=2/5$?) and SC_γ* ($q=1/3$) are also given in Fig. 8(a). So long as we adopt the Ising model, we can naturally explain not only the stable existence of these subphases but also the characteristic field dependence of their conoscopic figures. In other words, the existence of at least four such subphases prompted us to adopt not only the Ising model for the ferrielectric subphases but also the criterion for their identification by observing the electric field dependence of the conoscopic figures.

Two statistical mechanics models with Ising spins have been developed for illustrating the emergence of the devil's staircase.[10] The one with weak long-range forces is the one-dimensional Ising model[63,64] and the other with thermal fluctuations is the so-called ANNNI (axial next-nearest neighbor Ising) model with competing nearest and next-nearest neighbor coupling.[65,66] Isozaki *et al.*[46,47] explained the observed sequence of the subphases in terms of the Ising model with the long-range repulsive interactions, but Fukuda *et al.*[21] and Itoh *et al.*[50] pointed out several difficulties in the explanations. In particular, it is quite artificial to consider that the Ising spin represents not a real molecular tilting state (right or left) but the pair-state of two neighboring layers (synclinic or anticlinic), as Yamashita and Miyazima[12] pointed out when they tried to apply the ANNNI model to this problem. Their trial together with subsequent developments has been successful in explaining a wide variety of experimental facts. We now believe that the ANNNI model can describe the complicated phenomena under consideration most appropriately at least in the zero order approximation. In Fig. 6(b) are illustrated three rather simple molecular arrangements for the subphases with $q=2/5$, 2/7 and 1/5 in spr3, 2 and 1, respectively. Clearly, the molecular arrangements predict the melatopes appearing parallel to an applied electric field as already explained in SC_γ*. The plateaus due to the subphases in spr's are also observed, though not clearly, as illustrated in Fig. 8(b).[50]

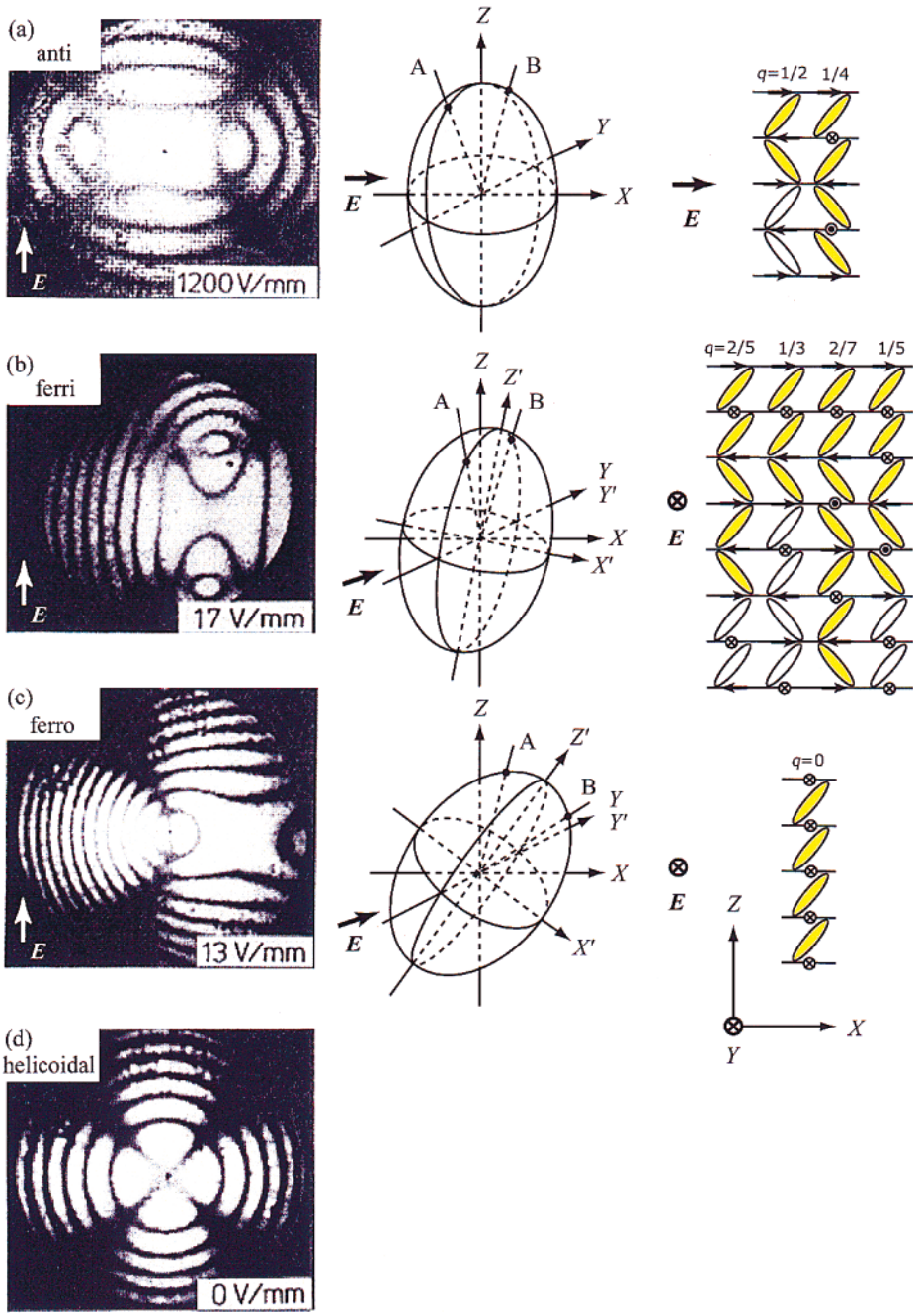

Fig. 6 Conoscopic figures under an applied electric field, indicatrix ellipsoids, and molecular alignments based on the Ising model.[21]

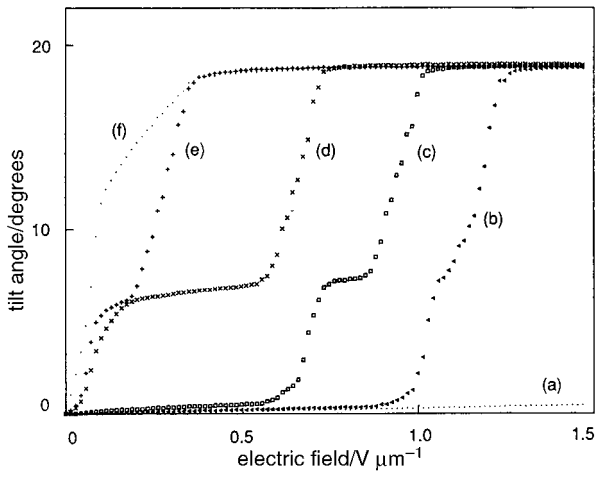

Fig. 7 Apparent tilt angles as a function of an applied electric field.[61]

3.3. Helicoidal structures clearly observed optically

Arun Roy and Madhusudana[67] insisted that the constituent molecules are chiral and the system is helicoidal, and hence that the XY model is more appropriate than the Ising model. Several investigators have, in fact, also made some explanations in terms of the XY model. Chiral interactions are usually small in comparison with achiral interactions. Cepic and Zeks[68] pointed out, however, that the next nearest neighbor antiferroelectric achiral interaction may cause a large azimuthal angle difference between molecular tilt directions in adjacent smectic layers. The model predicts a succession of commensurate and/or incommensurate structures in which the azimuthal angle difference between molecular tilt directions in adjacent layers is a fraction of 2π. Two such simple structures are shown in Fig. 9, which have three-layer and four-layer periodicities, respectively. When we try to correlate the three-layered structure to SC_γ^* and the four-layered one to AF, a difficulty arises. In some compounds, FI_L, SC_γ^* and AF were confirmed to have the helicoidal structure which is clearly

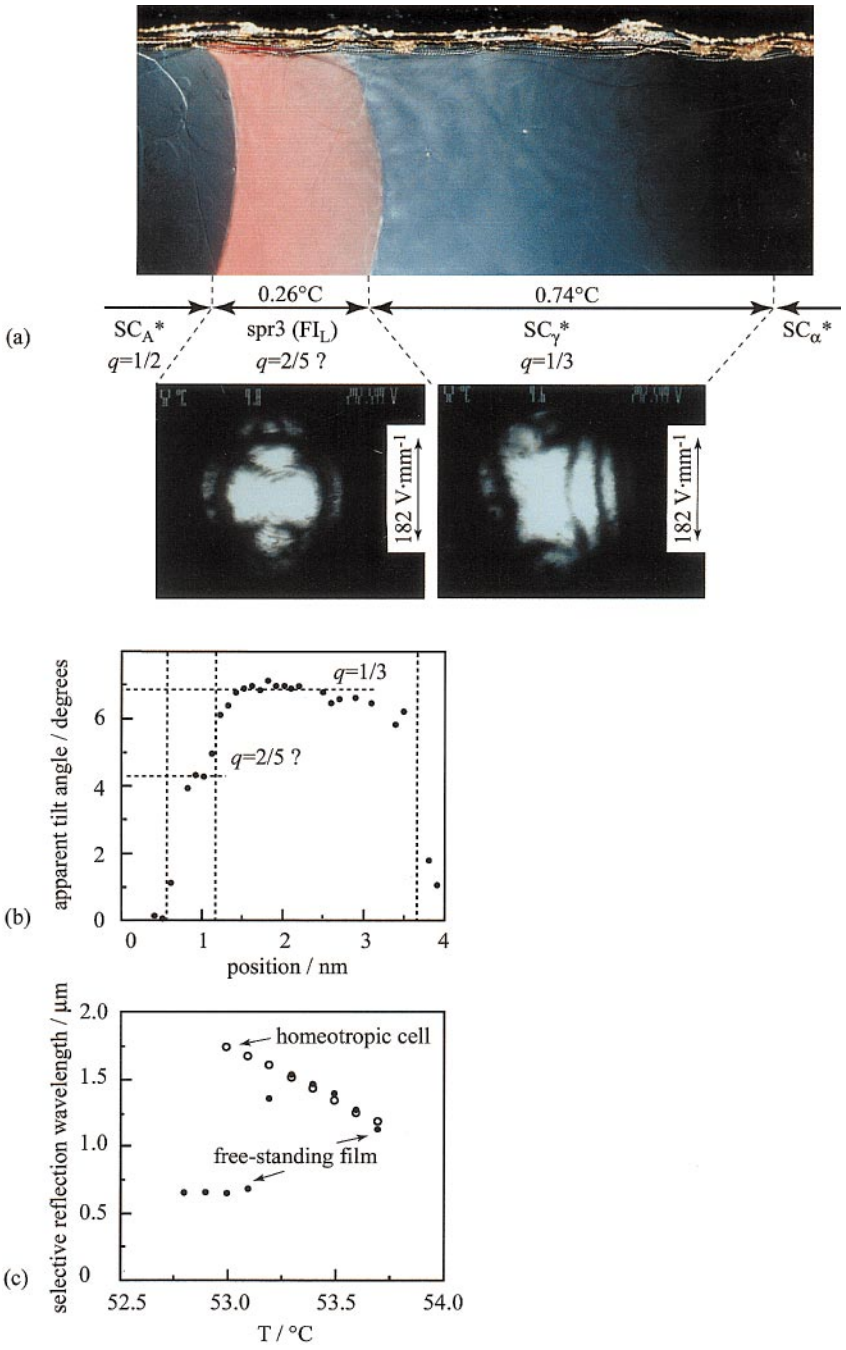

Fig. 8 A helicoidal ferrielectric phase in spr3 ($q=2/5$?) observed in compound **8**.[50] (a) A micrograph of a *ca.* 100 μm thick free-standing film under temperature gradient and characteristic conoscopic figures under applied electric fields in FI_L ($q=2/5$?) and SC_γ* ($q=1/3$); (b) Apparent tilt angle *vs.* temperature (position in the micrograph (a)) determined by measuring center-shift of conoscopic figures under an applied electric field; (c) Temperature variation of selective reflection peaks due to the FI_L and SC_γ* helicoidal structures; (d) Laser light diffraction patterns obtained at various temperatures in a 350 μm thick cell aligned homogeneously using a magnetic field. The patterns are shown at 0.1 °C intervals and their ordinate zeros are shifted upwards constantly by one division.

observed optically by characteristic reflection (laser light diffraction) optical rotatory dispersion, or circular dichroism, as illustrated in Fig. 8(c) and 9(b). The refractive index anisotropy detectable by light propagating along the helicoidal axis is as large as that in SC_A* and SC*. Consequently, the simple structures based on the XY model shown in Fig. 10 are not appropriate for SC_γ* and AF, because the symmetry around the helicoidal axis is equal to or higher than C_3 and no such refractive index anisotropy exists.

Introducing the much more complicated phenomenological free energy that contains six chiral and achiral interlayer interactions, Arun Roy and Madhusudana[69] obtained four subphases other than SC_A* and SC*. Fig. 11(a) schematically shows their structures at zero electric field. An applied electric field deforms the structures and produces the commensurate ones, which have in-plane spontaneous polarizations in a few numbered layers as illustrated in Fig. 11(b). Since the polarizations were considered to emerge perpendicular to the tilt plane, the field-induced structure that they proposed for SC_γ* is quite similar to the one in Fig. 6 based on the Ising model. Hence it can explain the melatopes appearing parallel to an applied electric field. When no field is applied, SC_γ* should be assigned to FI_I shown in Fig. 11(a). The helicoidal structure of FI_I may clearly be observed optically because of the large refractive index anisotropy due to the nonuniform modulation. Thus, at last, they were able to explain the optical and electro-optical properties of SC_γ*.

Experimentally, however, there exist at least three other

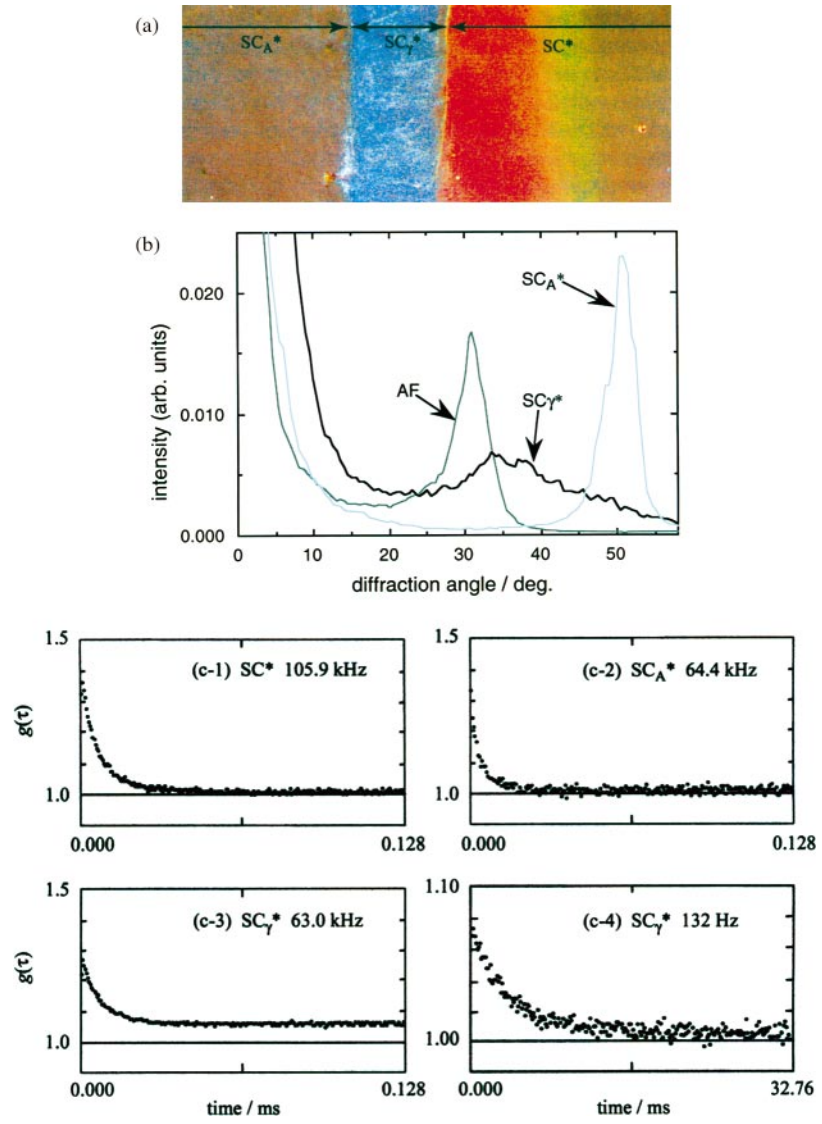

Fig. 9 Disordered and fluctuating character of SC$_\gamma$* ($q=1/3$).[70] (a) A micrograph of a 100 μm-thick free-standing film of compound **1** under temperature gradient; (b) Laser beam diffraction patterns of SC$_A$*, SC$_\gamma$* and AF in a 350 μm-thick homogeneous cell of compound **4**; (c) Intensity autocorrelation functions of (a) SC*, (b) SC$_A$*, (c) and (d) SC$_\gamma$* in a 100 μm-thick film of compound **1**.

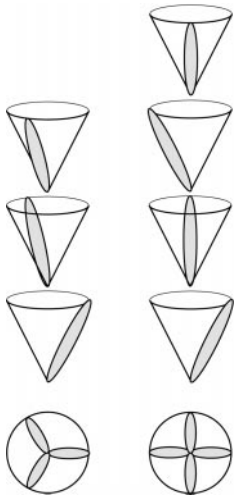

Fig. 10 Two simple molecular alignments based on the XY model, which have three layer and four layer periodicity, respectively.[68]

similar phases in spr3, spr2 and spr1, which have large refractive index anisotropy at zero field and the melatopes parallel to the field. Their free energy, though very sophisticated and complicated, could explain neither the properties of one of these subphases, FI$_L$ in spr3, nor the existence of the other two subphases, FI$_H$ and FI in spr2 and spr1. Moreover, the term $-\xi_i E$ in the phenomenological free energy does not correctly describe the interaction with an applied electric field, since the in-plane spontaneous polarizations are parallel to the tilt plane in SC$_A$* and perpendicular to it in SC* as illustrated in Fig. 2 and 6. The ANNNI model can solve these difficulties quite naturally. The resonant X-ray scattering experiment has unambiguously confirmed the exact anticlinic relation between adjacent layers in SC$_A$ and the approximate one in SC$_A$* together with a slight precession due to chirality.[4] There exists the short range intermolecular interaction that stabilizes the anticlinic relation between adjacent layers as described in Section 2.[11]

3.4. Disordered, fluctuating character of SC$_\gamma$* and Ising spin flipping

In this way, the ANNNI model appears to describe appropriately the subphases and the successive phase transitions under

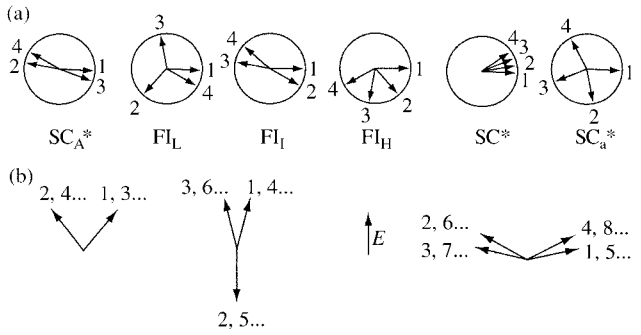

Fig. 11 Molecular alignments calculated by Arun Roy and Madhusudana[67,69] (a) for four subphases as well as SC$_A$* and SC* at zero electric field and (b) for SC$_A$*, FI, and SC$_\alpha$*.

consideration, at least in the zero order approximation. In this description, thermal agitations need to flip spins between the ± 1 states so that a variety of phases are certain to emerge, forming a devil's staircase. Spontaneous disorders and fluctuations caused by the flipping have been observed experimentally in SC$_\gamma$* as illustrated in Fig. 9(a)–9(c). Fig. 9(a) shows a disordered SC$_\gamma$* ($q=1/3$) structure even in a free-standing film of compound **1** and Fig. 9(b) gives laser beam diffraction patterns in SC$_A$*, SC$_\gamma$* and AF of compound **4**.[70] Three characteristic features of the SC$_\gamma$* pattern are: (1) the zero order diffraction peak due to the Rayleigh scattering is very broad; (2) the background is very high; and (3) the first order diffraction peak is very broad and sometimes has several subpeaks. These disordered features do not result from the cell quality but reflect the intrinsic properties of SC$_\gamma$*, because the diffraction patterns of SC$_A$* and AF that appear below and above SC$_\gamma$*, respectively, look quite normal. Fig. 9(c) shows intensity autocorrelation functions of scattered light in SC$_A$*, SC$_\gamma$* and SC* of compound **1**. In all these phases, the functions decay exponentially as illustrated in Fig. 9(c-1–3). The exponential decay is attributed to the Goldstone modes, *i.e.* the fluctuations of the helicoidal structures.[71,72] In SC$_\gamma$*, however, the function does not reach unity as seen clearly in Fig. 9(c-3). This fact indicates the existence of a very slowly decaying component, which is actually observed in the much longer time scale as shown in Fig. 9(c-4). The slow component of the intensity autocorrelation function indicates temporal distortion, while the characteristic features of the laser beam diffraction pattern show spatial distortion. Obviously, these tremendous distortions could not be explained by the ordinary fluctuations of the helicoidal structure, *i.e.* the Goldstone mode, but suggest that the SC$_\gamma$* phase structure itself must be distorted.

Miyachi *et al.* proposed a distortion mechanism based on the Ising model as given in Fig. 12.[70] In order to reduce the electrostatic energy, nature tries to cancel in-plane spontaneous

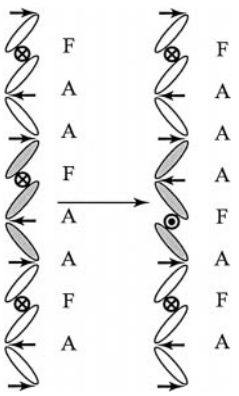

Fig. 12 A distortion mechanism of the SC$_\gamma$* phase structure based on the Ising model.[70] See text for details.

polarizations as locally as possible. The helicoidal structure in SC$_\gamma$* is not effective in neutralizing in-plane spontaneous polarizations spatially and reducing the Coulomb interaction energy, because its pitch is as long as 2 μm or more in compound **1**. In the unwound SC$_\gamma$* structure with $q=1/3$, in-plane spontaneous polarizations parallel to the tilt plane are neutralized, while those perpendicular to it add up to produce net ferrielectric spontaneous polarization. If one of the synclinic molecules flips as illustrated in Fig. 12, the in-plane spontaneous polarizations perpendicular to the tilt plane are also neutralized as is also shown there. Such flipping may easily occur thermally, because it does not change the number of the anticlinic (A) and synclinic (F) orderings of adjacent layers and because the formation energy difference between them is very small. Soliton-like mismatches must be thermally excited here and there, and some of these mismatches are pinned by surfaces and other defects, causing the dynamic and static distortions of the SC$_\gamma$* phase structure as well as its helicoidal structure. When the helicoidal pitch is short, the disordered character may disappear. A free-standing film of compound **8** gives uniform textures in not only SC$_\gamma$* but also FI$_L$. It shows coloring due to the characteristic reflection of their helicoidal structure, as seen in Fig. 8(a). Since the formation energy difference between the anticlinic and synclinic orderings of adjacent layers is smaller, the system becomes softer with respect to the tilt directions and hence substrate interfaces may more easily disturb the phase structures. In fact, as shown in Fig. 8(d), laser light diffraction patterns indicated the disordered features described above and the existence of SC$_\gamma$* and FI$_L$ was not confirmed in a homogeneous cell. Even in a homeotropic cell, as clearly seen in Fig. 8(c), the interface effects made it difficult to confirm the presence of FI$_L$.

The disordered character of SC$_\gamma$* discussed above suggests an important role played by the azimuthal angle freedom. However, this fact does not simply mean that the XY model is much more appropriate to describe the phenomena under consideration than the Ising model is. Since the $q=1/3$ structure based on the Ising model appears to be stabilized by an applied electric field as shown in Fig. 6, the ANNNI model still describes the phenomena appropriately at least in the zero order approximation. Conversely speaking, the disordered character of SC$_\gamma$* explained above experimentally ensures that the Ising spin may flip between the ± 1 states by using the azimuthal angle freedom and hence that its averaged value may become $\langle s_i \rangle = 0$. Here the Ising spin s_i represents the tilting sense of a local in-plane C-director but not of a single molecule.

3.5. Interplay between phase structures and helicoidal structures

As the pitch shortens further and the phase structure becomes more complex, the Ising model may not describe the system appropriately even in the zero order approximation. Suppose FI in spr1 has the $q=1/5$ phase structure of five layer periodicity and shows the characteristic reflection at 500 nm due to the helicoidal structure of *ca.* 350 nm pitch. Since the smectic layer spacing is *ca.* 3.5 nm, only 20 phase structural units are contained in a full helicoidal pitch and the azimuthal angle precesses 18° from unit to unit. The precession is so large that we could not neglect it. We have to treat both the structures at the same time. Some examples were observed in two component mixtures of compounds **9** and **10**. The temperature–mixing ratio (T–x) phase diagram[73] is obtained using free-standing films and is shown in Fig. 13. Phase identifications were made only by conoscope observation under an applied electric field. The phase boundaries were not distinct in mixtures in which the proportion of compound **10** is more than 50 wt%. The antiferroelectric phase was assigned as AF because of the existence of a ferrielectric phase (designated as

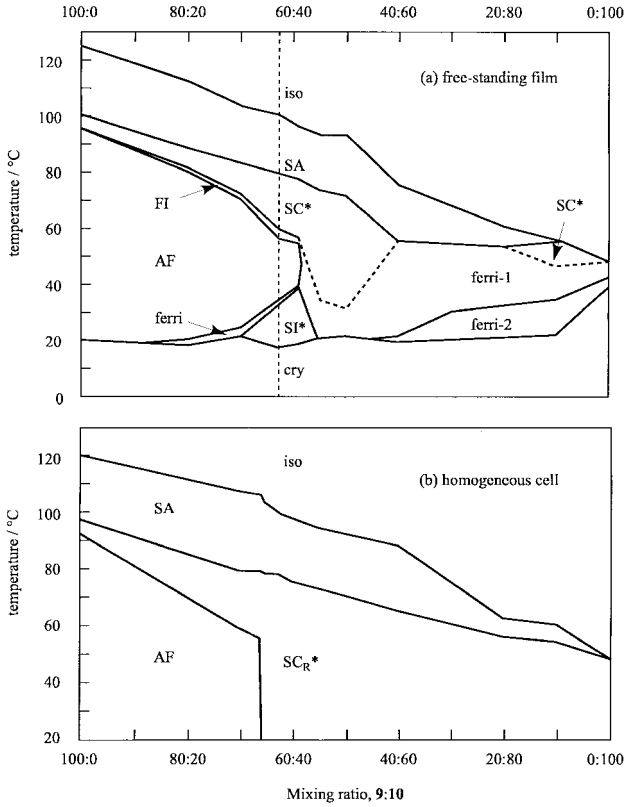

Fig. 13 Temperature–mixing ratio (T–x) phase diagram of compounds **9** and **10** obtained (a) using a free-standing film and (b) using a homogeneous cell.[73]

ferri in the phase diagram) on the low temperature side. The rather short pitch of 700 nm or less, however, suggests SC_A* instead of AF, since the subphases between SC_A* and SC* usually have long pitch due to the competition of SC_A* and SC* twisting powers with opposite handednesses.§

An interplay between phase structures and helicoidal structures[73] is observed in mixtures **9**:**10** = 50:50, 40:60 and 30:70 as shown in Fig. 14(a)–14(c). The temperature dependence of the pitch shows slight discontinuous changes at 51 °C in **9**:**10** = 40:60 and 48 and 53 °C in **9**:**10** = 30:70. These pitch jumps must be caused by the phase structural changes. Another irregular helicoidal pitch behavior was observed in the characteristic reflection spectra of a mixture **9**:**10** = 40:60 as illustrated in Fig. 14(d). Both half and full pitch reflection bands show splitting. In SC_A*, the splitting of half-order diffracted peaks due to the helicoidal structure was detected in the resonant X-ray scattering,[4] but no splitting was observed in the selective reflection due to the helicoidal structure. The double layered SC_A* phase structure must be too simple to cause any observable splitting in the selective reflection peaks. It is quite natural to consider that more complex phase structures with small wavenumbers (q's) may cause some splitting, which is in fact observed in Fig. 14(d). The temperature dependence of helicoidal pitch appears to be continuous in **9**:**10** = 50:50, although we confirmed the conoscopic figures under applied electric fields characteristic of SC* in the high temperature region but those characteristic of ferrielectric phases in the low temperature region. The difference in conoscopic figures between the high and low temperature regions is very small and the helicoidal pitch does not show any discontinuous change between SC* and a ferrielectric phase.

Moreover, the electric field dependence of conoscopic figures in the ferrielectric phase is also quite continuous as observed in a mixture of **9**:**10** = 50:50.[73] Fig. 15(a) shows the electric field dependence of conoscopic figures at 24, 26 and 28 °C. We can clearly see the ferrielectric-like conoscopic figures with melatopes parallel to the field at about 150 V mm^{-1} and the ferroelectric-like ones with melatopes perpendicular to the field at 250 V mm^{-1}. Using the center of the conoscopic figures at 28 °C, we obtained the apparent tilt angle as a function of applied field; the result is given in Fig. 15(b). The apparent tilt angle shows no threshold field and increases continuously. Although the maximum tilt angle of about 25° was not attained at the highest field used in this experiment, the change from ferrielectric-like (at about 105–150 V mm^{-1}) to ferroelectric-like is included in Fig. 15(b). Almost continuous emergence of a variety of commensurate and/or incommensurate phase structures, we believe, causes these temperature- and field-induced continuous changes from ferrielectric to ferroelectric phases. The emergence may occur because the mixtures become so soft with respect to the tilt directions that the anticlinic and synclinic orderings of adjacent layers have almost the same formation energy so that the azimuthal angle fluctuations are very large. The extreme softness makes the interface effect much more drastic. The temperature–mixing ratio (T–x) phase diagram in a thin homogeneous cell is quite different from that in a thick free-standing film as illustrated in Fig. 13. Since so-called V-shaped switching is observed, the details will be described in Section 5 later.

Regarding the emergence of a variety of commensurate and/or incommensurate phase structures, compound **11** is worthy of attention, which is a component of the Inui mixture, **11**:**12**:**13** = 20:40:40, showing V-shaped switching.[74a] Fig. 16(a) illustrates the temperature dependence of the wavelength of the selective reflection peaks observed in normal and 30° oblique incidence using compound **11** free-standing film of about 100 μm thickness. The full pitch band was confirmed only in the low temperature region, and the helicoidal pitch diverged at about 50 °C. The conoscopic figures under an applied electric field indicated that the phase is ferrielectric both in the high and low temperature regions. The conoscopic figures could not be observed in the middle temperature region where the helicoidal pitch diverges. The tilt angle and spontaneous polarization are very large, 41° and 2.6 mC m^{-2} (260 nC cm^{-2}), respectively, which were measured in SC* by applying a high enough electric field using a homogeneous cell. An anomaly was observed only at the SA–ferri transition by high precision ac calorimetry.[75] Apparently, a single ferrielectric phase emerges in the temperature range as wide as more than 100 °C. Sensitivity to interfaces is also drastic, and V-shaped switching is observed in the homogeneous cell, as will be explained in Section 5. Whether it is really a single phase is a future problem. We suspect an almost continuous emergence of a variety of commensurate and/or incommensurate phase structures. Fig. 16 also shows the temperature dependence of the characteristic reflection peaks in three additional similar compounds, **14**, **15** and **16**,[74b] where a single ferrielectric phase apparently emerges in the wide temperature range, together with that in compounds **12** and **13**.

4. Studies based on theoretical models

4.1. Ising model or XY model?

As new aspects of the phenomena were observed, various types of phenomenological theories have been introduced to clarify these. First, the bilayer model was introduced by Orihara and Ishibashi[13] and generalized by many authors,[14,68,76–81] *e.g.*, the three and four layer model[80] and

§Suppose the ferrielectric phase on the low temperature side is the SI*-like ferrielectric one, it is possible to assign the antiferroelectric phase to SC_A*. As will become clear in Subsection 4.2, however, this assignment may not be probable. Since a variety of phases appear as the mixing ratio changes, the antiferroelectric phase should be AF (q = 1/4).

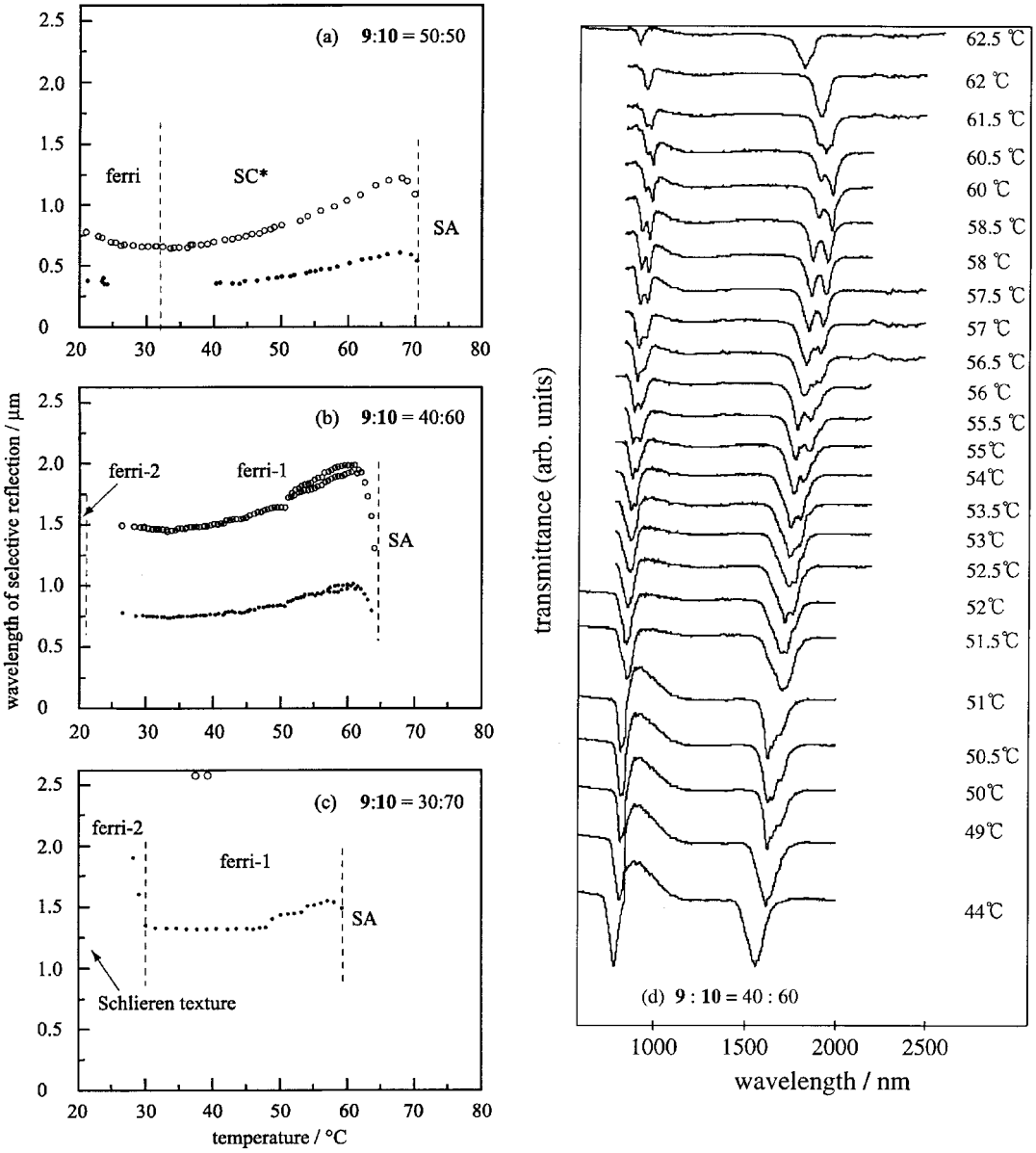

Fig. 14 Temperature dependence of the pitch observed in mixtures of (a) **9**:**10** = 50:50, (b) 40:60 and (c) 30:70. Characteristic reflection spectra of a mixture **9**:**10** = 40:60 are also given in (d). Note slight discontinuous changes in (b) and (c) and the splitting of characteristic reflection peaks in (b) and (d).[73]

the multilayer one.[77,81] However, those models are essentially based on the XY model and the concept of the devil's staircase, suggested from the experimental facts, is neglected, while such a concept has been stressed from an early stage of the observations of the relevant phenomena as mentioned in the preceding Section.[6,21,50] Stimulated by this assertion, studies on the successive phase transitions were reported in 1993 on the basis of the Ising model.[12,86] In the present stage, it is required to explain the phenomena as a whole on the basis of a concrete model.

From the symmetry of those phases, the tilt of the molecular long axis may take any direction, and hence the system can be described by a model like the classical Heisenberg model, where a change of the tilt angle is taken into account. In practice, the variation of the tilt angle is surely important in SC_α*. However, in the sequence of phase transitions between SC* and SC_A* shown in Fig. 5, the tilt angle is sufficiently large and its change can be neglected as far as the mechanism of the successive phase transition is concerned. From the conoscopic observations of those phases mentioned in Section 3.2, the tilt direction is in one coplane which is twisted with the helicoidal structure of the system. Consequently, the orders of those phases belong to an Ising class, and the system can be described by the Ising model.[6,12,21,46–50,82–89] Here it is pointed out that the ferroelectric phase SC* appears in the high temperature region while the antiferroelectric phase SC_A* is always located in the low temperature region, and between these various mesophases appear.[6,12,21,46–50] This fact suggests that the origin of the successive phase transitions is competition, or frustration, between interactions of opposite types which stabilize the respective phases conflicting mutually.

Following such considerations as mentioned above, Yamashita and his collaborators have introduced the generalized ANNNI model to explain the successive phase transitions, where the tilt direction of the i-th molecule is described by a spin variable s_i $(=1, -1)$.[12,82–85] Their Hamiltonian is given by eqn (1).

$$H = -J\sum_{i,j} s_i s_j - J_1 \sum_i^A s_i s_{i+1} - J_2 \sum_i^A s_i s_{i+2} - J_3 \sum_i^A s_i s_{i+3} \quad (1)$$

Here J is the interaction parameter between the nearest neighboring pairs and the first summation Σ is taken all over the nearest neighboring pairs (i, j) in the same layer; the other

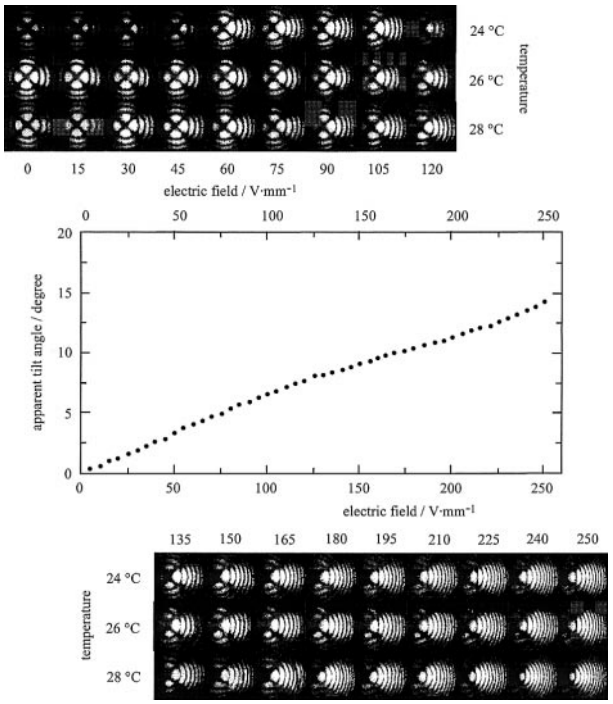

Fig. 15 Continuous change from ferrielectric to ferroelectric as observed in a mixture of **9**:**10** = 50:50 (a) the electric field dependence of conoscopic figures at 24, 26 and 28 °C and (b) the apparent tilt angle as a function of applied field determined by using the center of the conoscopic figures at 28 °C.[73]

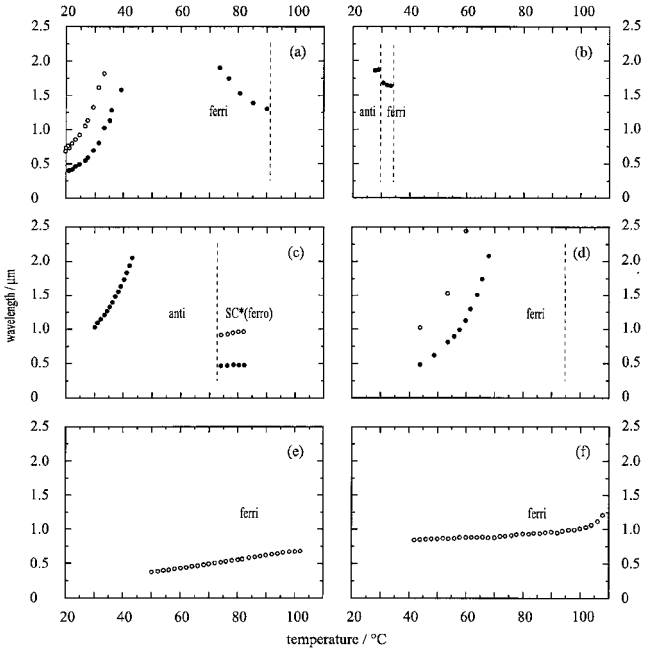

Fig. 16 The temperature dependence of the characteristic reflection peaks observed in 30° oblique incidence using free-standing films of about 100 μm thickness in compounds (a)–(f), **11**–**16**.[74a,b] Open circles are for the so-called full-pitch band reflection, which is not obtained in normal incidence.

summations Σ^A are only over the first, second and third neighboring pairs of the axial direction parallel to the smectic layer normal. In the original ANNNI model,[65,66] the energy parameter J_1 denoting the nearest neighbor interaction in the axial direction is transformed to the one with opposite sign, $-J_1$, by the local gauge transformation, s_i to $(-1)^k s_i$, where k denotes the number of the layer to which s_i belongs, and accordingly we have only to consider the positive (or negative) side of J_1. On the other hand, in the successive phase transitions of antiferroelectric smectic liquid crystals, the wave number of phases changes from SC* ($q=0$) to SC_A* ($q=1/2$) and the parameter J_1 should be extended to take a whole range of values.[12] In addition to this, the third nearest neighbour interaction J_3 in the axial direction[90] is to be taken into account in that model in order to stabilize SC_γ*, because the phase SC_γ* is as important as AF in the sequence of phases in Fig. 5.[12,21,46,47,50] Of course, the symmetry with respect to J_1 mentioned above is violated by the existence of J_3 and the extension of J_1 is necessary. Anyway, it should be stressed that the extension of J_1 leads to one of the essential concepts in the successive phase transitions of antiferroelectric smectics under consideration, which will be mentioned in the following Subsections.

We have other approaches to explain the phenomena using various types of XY model, which are, to a greater or lesser extent, the generalization of the preceding phenomenological theories.[13,14,68,76–80] On the basis of these models experimental data are fitted in detail,[69,91] but the general properties of successive phase transitions are not explained as mentioned in Subsection 3.3. In these XY models the competing second nearest neighbour interaction J_2 is also essential together with various types of forces.[67–69,78,91–93] In this respect, the long range character of interactions and the frustration between those are common to the approach based on the generalized ANNNI model. A recent experimental investigation on the structures of some mesophases by means of resonant X-ray diffraction suggests applicability of the XY model,[4,¶] although the result is in opposition to the helicoidal structure and the conoscope observation mentioned in Subsections 3.2 and 3.3. At any rate, the investigations based on the XY model are also useful, nevertheless the general features of the mechanism of successive phase transitions are clarified not by this model but by the ANNNI model. The Ising model is too simple to be applied to the quantitative investigation of the widespread of phenomena of various types of species, and also to a certain kind of dynamical problem as mentioned in Subsections 3.4 and 3.5. In this respect both approaches are complementary to each other.

4.2. Phase sequences and parameter values in the Ising model

In the application of the model to the present problem, the parameter J_1 is considered to have an electrostatic origin and a steric one, and accordingly is expressed as eqn (2),

$$J_1 = -J_0 + TS \qquad (2)$$

where J_0 and S are positive constants and T is the temperature.[12] On the T–J_1 phase diagram of the generalized ANNNI model, J_1 has the locus according to eqn (2) as T changes. The point at which J_1 crosses the coexisting curve corresponds to a phase transition and the sequences of such points show the successive phase transitions, from which the general features of successive phase transitions are explained naturally.[12,50,82,83] Optical and electro-optical observations are also explained by this model as mentioned in Subsections 3.2 and 3.3. In addition, unknown phases between SC* and AF, *i.e.* in the spr1 region in Fig. 5, are predicted[12] and this is confirmed by the subsequent observation of FI.[48–50] This fact also supports the applicability of the present model to the phenomena under consideration. Up to now, one subphase has been proved definitely in each subphase region, spr1, spr2 and spr3. The observation of additional new subphases in the vicinity of FI_L and FI_H[46] is quite interesting, because the present model leads as well to the possibility of such new subphases. As for the structures of the mesophases, FI_L is

¶As far as the scattered intensity is concerned, the very small half-order satellites appear to support the antiferroelectric SC_A*($q=1/4$) structure shown in Fig. 6. The small intensity may result from the helicoidal structure. Detailed study of the polarization characteristics of the scattered intensity will solve the problems.

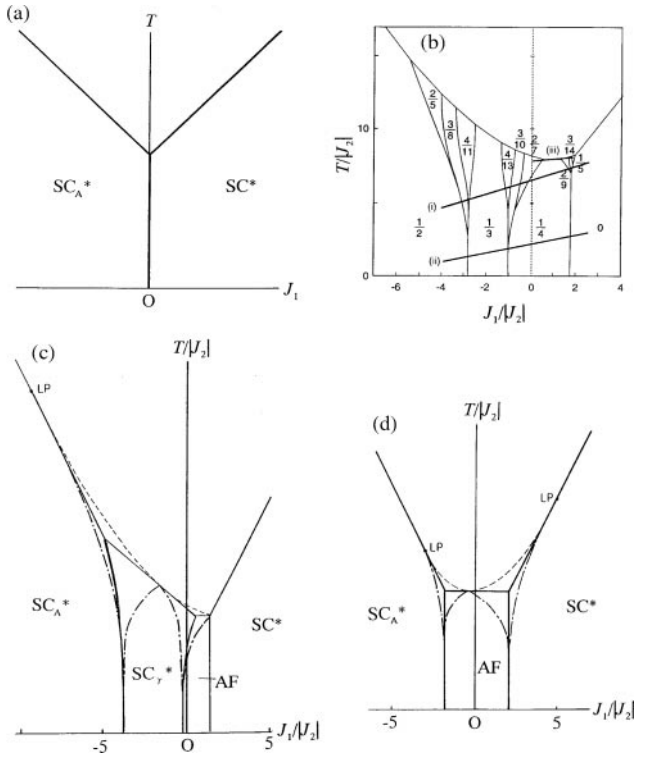

Fig. 17 The T–J_1 phase diagram of the Hamiltonian eqn (1); (a) $J_2=J_3=0$, (b) $J_3/|J_2|=0.3$, (c) $J_3/|J_2|=0.6$, (d) $J_3/|J_2|=-0.1$, where figures (c) and (d) are drawn schematically.[12]

identified as having the wave number $q=2/5$ by comparing the values of the order parameters with the behavior of the apparent tilt angle,[50,82–84] and FI_H is supposed to have 2/7 from the similarity of the behaviours in the electric field to FI_L.[85]

As mentioned in Subsection 3.1, all of the mesophases do not always appear in each material. Here, a general feature of the relationship between the set of parameter values and the appearance of phases is reviewed.[12,82] Four typical T–J_1 phase diagrams are shown in Fig. 17(a)–17(d). If the second and third nearest neighbour interaction parameters, J_2 (<0) and J_3, are negligibly small as compared with the interaction parameter between the nearest neighbouring pairs in the same layer, J, the first order transition from SC* and SC_A* directly occurs and no mesophase is observed as shown in Fig. 17(a). The transition temperature is given by $T_c=6J\pm2J_1$. On the other hand, in the case where the magnitude of J_2 amounts to a value of, say, an order of $J/10$, the successive phase transitions occur.‖ In Fig. 17(b) representative loci of J_1 are shown with labels (i) and (ii). As for the magnitude of J_3, a stable range of SC_γ* is comparable to the one of AF for $J_3/|J_2|\cong0.3$, and the phase transitions, SC*–AF–SC_γ*–SC_A*, occur. As J_3 increases, SC_γ* is stabilized and enhanced, *i.e.* the sequence of phases, SC*–SC_γ*–SC_A* is expected to appear. In practice AF disappears in the ground state for $J_3/|J_2|>1.0$. Fig. 17(c) is the phase diagram at $J_3/|J_2|=0.6$, in which the stable range of AF is quite narrow. On the other hand, for a small value, or negative value, of J_3, the sequence, SC*–AF–SC_A*, occurs as shown in Fig. 17(d). The appearance of subphases, FI_L, FI_H and FI, depends mainly on a ratio J_0/S, corresponding to the intersection of J_1 given by eqn (2) with the T-axis. For suitable value of J_0/S, these phases are expected to appear as illustrated by line (i) in Fig. 17(b), while for small values of J_0/S, these are hardly observed as shown by line (ii) in Fig. 17(b). It is noted that in the limit of the vanishing values of J_2 and J_3, all the stable regions of mesophases shrink and disappear and phase diagrams (b), (c) and (d) are reduced to the one shown in (a). In case the intersection is close to the critical line of the present model, separating the modulated phase from the disordered one, the order is fairly small. It is susceptible to factors that we disregard here, such as the effect due to a boundary, which will be discussed in the next section in relation to the V-shaped response.

‖One may criticize that $J_2\approx J/10$ is too large. As will be explained in detail in Subsection 4.4, however, the Ising spin s_i is not for a single molecule but for the local in-plane C-director. Consequently, a considerably large distortion may occur even within a single layer.[94–96]

4.3. Origin of the long range interactions

An effect due to a dipole moment has been stressed from an early stage of investigation after the discovery of the SC_A*.[21,31,37] Because the dipole moment is attached towards the end part of the molecule,[23–30] the freedom of sense of the molecular long axis is considered to be one of the important variables,[21,37,87–89] nevertheless it is barely observed. Such a variable is a candidate for the origin of the long range interactions introduced in the model mentioned above.

Let the variable t_i take the values 1 and -1 denoting the up or down sense of the long axis. Then, the energy of the system is written as eqn (3),

$$H=-J\sum_{(i,j)}s_is_j-J_1^{(0)}\sum_i^A s_is_{i+1}$$
$$-\sum_i^A\{(E_1s_is_{i+1}+E_3)t_{i+1}+E_2s_i(s_{i-1}-s_{i+1})\}t_i \qquad (3)$$

where three energy parameters E_m ($m=1$, 2, 3) are given as linear combinations of six parameters representing the six configurations of pair states, shown in Fig. 18(a). By summing over all states of t_i preserving s_i in a variable at the partition function, effective long range interactions such as J_2 and J_3 are induced[97] and the negative definiteness of J_2 is certified.[97–99] We can easily see the mechanism of the negative definiteness of J_2 by testing a typical case, where $E_1=E_3=0$.[100] Then, the decimation transformation about t_i is written with k_B the Boltzmann constant as in eqn (4).

$$\sum_{t_i=\pm1}\exp\{E_2(s_{i-1}-s_{i+1})/k_BT\}=2\,\mathrm{ch}\{E_2(s_{i-1}-s_{i+1})/k_BT\} \qquad (4)$$

By rewriting the right hand side of eqn (4) in the form $c\exp(J_2s_{i-1}s_{i+1}/k_BT)$, J_2 is obtained explicitly in eqn (5),

$$J_2=-\frac{k_BT}{2}\ln\mathrm{ch}\frac{2E_2}{k_BT} \qquad (5)$$

where the negative definiteness of J_2 is apparent. General cases are studied numerically, and as well are supported by an analysis of the ground state of Hamiltonian (3) irrespective of the decimation transformation, where AF and SC_γ* are stable in each respective region.[98,99]

In place of the freedom of sense of the molecular long axis, we can introduce the rotational freedom about the molecular long axis,[98,99] which is supported by the following experimental fact that the direction of the dipole moment is confirmed to be in the tilt plane at SC_A* while it is in a direction perpendicular to that plane at SC*.[31–35,98,99] In practice, the change of the rotational state is assumed to take place more easily than the head–tail change. If the above interpretation that such a rotational state is restricted to two orientations as shown in Fig. 18(b), then the analysis to induce the long range interactions mentioned above is applied to this freedom without any additional change by only interpreting the variable t_i to denote the two rotational states.[98–100] Since the rotation takes place continuously, this interpretation is correct only if the

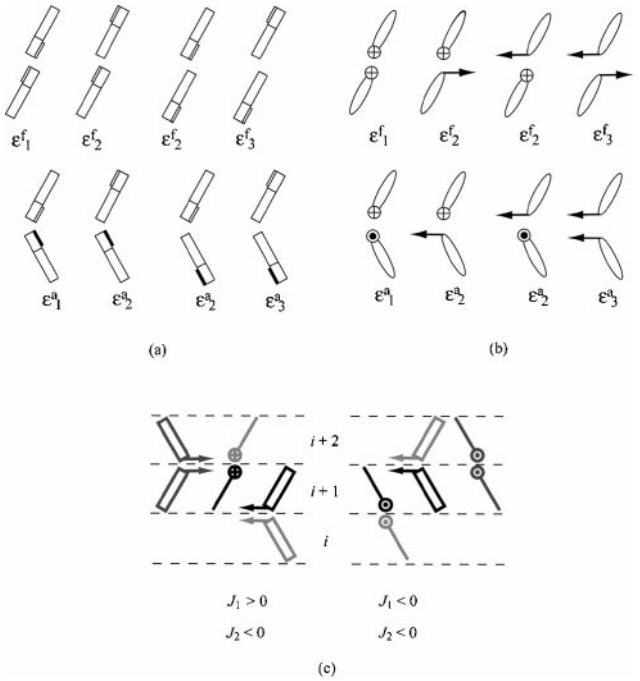

Fig. 18 The assignment of the energy parameters (a) for the head and tail pair states and (b) for the pairs of molecular rotation about the long axis.[97] The interaction in a single layer may also be important as illustrated in (c).

direction of the dipole is restricted to two such directions at the thermal equilibrium.**

In consideration of the effect of the dipole moment, nevertheless, the freedom of the sense of the long axis is surely relevant to the present phenomena, because the dipole is attached to the end part of each molecule and related strongly to the pair state of neighboring molecules. We have other configurations besides those shown in Fig. 18(b), where configurations with low energies are selected and picked out. Thus, each of the freedoms, sense of molecular long axis and rotation around that, should not be ignored and considered to work cooperatively as an origin of the long range interactions in case we utilize the tilt direction exclusively as an independent variable to describe the system.

It is noted here that the competition occurs in a double sense; the first one is the frustration coming from J_1 and J_2 and the second one is the two different origins of J_1 expressed explicitly in eqn (2). We have learned a mechanism of successive phase transition symbolized in terms of the devil's staircase occurring due to the frustration between J_1 and J_2 in such simple models as the ANNNI model. On the other hand, phenomena occurring in ferroelectric and antiferroelectric smectics directed our attention to the competition between interactions in J_1 as described in eqn (2). In general, indirect long range interactions discussed here are not so strong, while the fundamental one in J_1 is weakened here, and eventually competition between J_1 and J_2 occurs. It should be stressed that all of the mesophases between SC* and SC_A* appear in the area where the magnitude of J_1 is small. Both the frustration and the competition of interactions are essential in the phenomena under consideration. In the following Section the V-shaped response of transmittance of light to the electric field is explained, which is quite sensitive to the boundary condition. This phenomenon is also attributed to the smallness of J_1 in cooperation with the frustration.

The mechanism to bring J_2 into the XY model is presumed to be essentially the same as the one derived explicitly in the Ising model as mentioned above, though it is not easy mathematically to induce J_2 because of the continuous range of values the XY variable takes. This is an open question to be solved in the future.

4.4. Unification of Ising and XY models

As mentioned above both Ising and XY models are complementary in describing the whole phenomena observed in ferroelectric and antiferroelectric smectic materials. Both models are extreme ones and a certain model between these may describe each real material. So, it is interesting how both characters of each model are connected. Here, the XY model with competing interactions J_1 and J_2 exposed to a two fold field H has been introduced, which is reduced to the ANNNI model in the limit of an infinitely large magnitude of the field.[101]

In Fig. 19 an outline of the phase diagram in T–J_1–H space (in the unit of $|J_2|$) is shown, where in the plane $H=0$, the modulated phase changes continuously while in the plane $H=\infty$, the devil's staircase of the ANNNI model is sketched. In the ground state, the freedom of the XY spin is frozen at fairly small magnitude $H_c=0.75$, and only in a part of the region $H<H_c$, the freedom of XY spin survives as shown in Fig. 19.[101,102] At finite temperatures,[103] on the other hand, the order of Ising symmetry appears first at high temperatures, T_c, even in the region where the freedom of XY spin survives at $T=0$. The relation of the wave number of the phase appearing at T_c to the value $J_1/|J_2|$ is irrespective of the value of H, and eventually common to the XY model and to the ANNNI model as well. At a temperature T_c' lower than T_c,

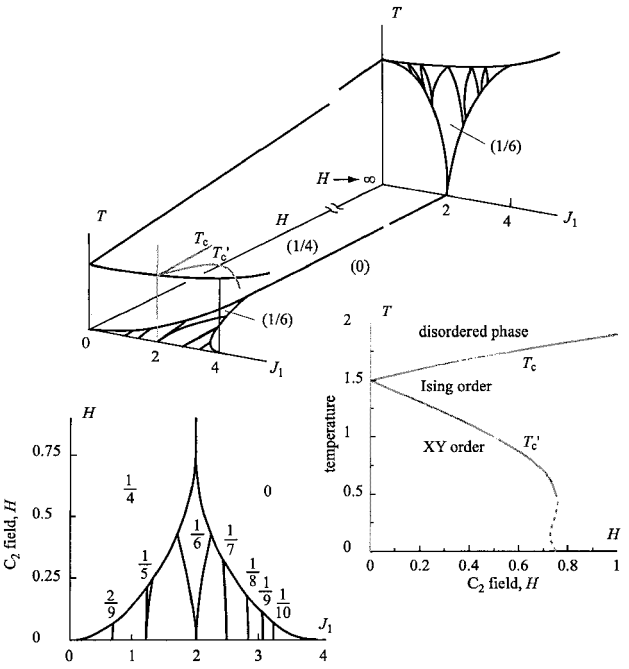

Fig. 19 Sketch of the phase diagram showing the crossover from XY to ANNNI model.

**Once this rotational freedom is taken into account, the interaction in a single layer may also be important as illustrated in Fig. 18(c). The chiral chain of a molecule under consideration is bent with respect to the core, as illustrated in Fig. 1. Moreover, the averaged shape of the core is not cylindrically symmetric in ferroelectric SC* and antiferroelectric SC_A*. For example, the biased direction of the phenyl rings is more or less perpendicular to the tilt plane in SC*; this is in contradiction to the initial speculation by Meyer, but is always in accordance with the electric field dependence of the conoscopic figures. The chiral chain is assumed to be coplanar with the averaged phenyl ring plane. Then the molecules are schematically represented as shown in Fig. 18(c). Although the rotation about the molecular long axis is biased to some exent, the degree of bias is not so large. Hence a tendency still exists that the rotational distribution may become cylindrical. This means that there is a tendency $J_2<0$ as is clear in Fig. 18(c).

the freedom of XY spin begins to emerge macroscopically and the phase is confluent to the one in the ground state. The profiles of the probability distribution of the XY spin φ_i indicating the azimuthal angle of tilt direction are shown in Fig. 20.[103] These results show that the freedom of XY spin is suppressed strongly and appears only in the extremely restricted region, with low field and low temperature. It is noticed that in this region, a sort of fractal structure preserving the XY properties appears, though the predominance of commensurate phases except for the phase with $q=1/6$ is too small to be observed. Details of phase boundaries of this model are to be clarified in the near future, and also a model with interaction of the biquadratic type in place of the two-fold field is left as a future problem to be studied.

Let us consider whether the Ising spin, s_i, refers to a single molecule or a smectic layer. In order to have a devil's staircase in eqn (1), thermal agitations need to flip spins between the ± 1 states. In an actual process of the flipping, molecules may rotate their azimuthal angles, keeping the polar angle constant, around the smectic layer normal. Otherwise a change in the smectic layer spacing may occur, which costs too much distortion energy. Since its orientational order parameter is $S\sim 0.7$ or larger in fluid smectic SC* and SC_A*, however, a single molecule hardly flips individually. A group of molecules may rotate in a smectic layer in order to make the resulting distortion energy as small as possible. It is appropriate to consider that the Ising spin s_i representing the tilting sense, right or left, is not for a single molecule but for the local in-plane C-director in the ith smectic layer. Thus we can easily envisage the flipping and the state of its zero average value, $\langle s_i\rangle \sim 0$.

For a given temperature $\Sigma_i s_i/n$ takes a value $\langle s_i\rangle$, or $-\langle s_i\rangle$, where $\langle s_i\rangle$ is an average of s_i and n the number of particles belonging to the group. In practice, the thermodynamic potential is of the form of double minimum type in the ordered phases, and the minimum is steeper as n is larger. By regarding

$$\sum_i s_i/n\langle s_i\rangle$$

as a new spin variable which takes 1 and -1, then the analyses based on the ANNNI model mentioned in this section are valid so long as $\langle s_i\rangle$ is considered to be a constant, not so small value, in which all energy parameters are regarded as functions of temperature.[104,105] The thermodynamic potential is mapped in a similar form to the original one by this change of variable and the temperature is transformed to a higher one than the original temperature.[106] This interpretation is valid and useful conceptually and practically in the case where the change of $\langle s_i\rangle$ can be neglected, and accordingly applicable not to a global range of areas but to the local, *e.g.* to phenomena driven by the electric field. In fact, Yamashita and Tanaka[84] obtained the E–J_1 phase diagram illustrated in Fig. 21. They added in eqn (1) an additional term describing the interaction with an applied electric field, $-E\Sigma_i s_i$. Fig. 21 indicates two interesting facts: (1) the electric field stabilizes $q=2/5$ and $q=2/7$ phases in spr3 and spr2, respectively; and (2) the second order phase transition can occur under suitable conditions although the transition is necessarily first order in the absence of the electric field.

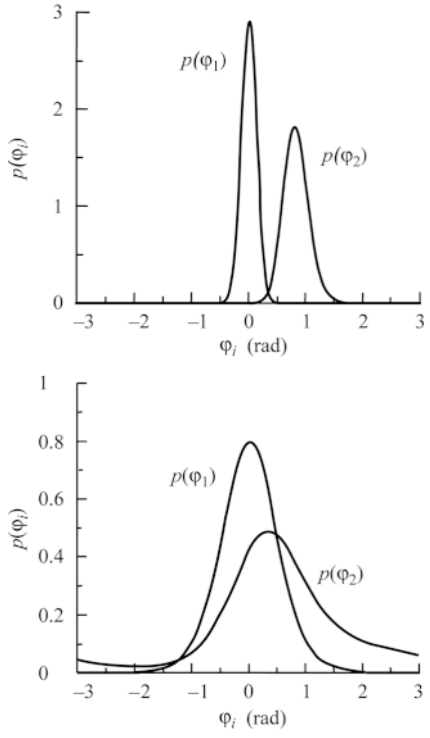

Fig. 20 Profile of the probability distribution of the azimuthal angles φ_1 and φ_2 at a phase with $q=6$, where $J_1=2$, $H=0.4$, $T/T_c'=0.091$ in (a) and 0.91 in (b).[103]

5. V-shaped switching

5.1. Thermally fluctuating local in-plane spontaneous polarizations at smectic layer boundaries

Ordinary antiferroelectricity in liquid crystals is characterized by the tristable switching observed in visible light transmittance under crossed polarizers with one of the axes parallel to the smectic layer normal. It is the electric-field-induced transition between antiferroelectric and ferroelectric phases and shows a conspicuous dc threshold and hysteresis together with a pretransitional phenomenon.[1,15] More than 1000 compounds that exhibit antiferroelectric and related liquid crystal phases have been synthesized because of their potential applications to displays.[107] The constituent molecules of all these compounds are considered to have the bent chiral chain.[23–29] As explained in Sections 3 and 4, these compounds are characterized by softness with respect to the tilting directions and senses between adjacent smectic layers and in a single layer. A compound is represented by a straight line, eqn (2), in a T–J_1 phase diagram based on the ANNNI model.[12] As the line approaches the second order critical curve, the system becomes softer. Two essential factors that determine the softness are the intermolecular interactions stabilizing SC_A* and SC* discussed in Section 2. In addition, the azimuthal angle fluctuations play an important role near the critical curve, on which the averaged value of Ising spins becomes zero, $\langle s_i\rangle=0$. When compounds are really hard, only SC_A* and/or SC* emerge. As they become soft, first SC_γ*($q=1/3$) and/or AF($q=1/4$), and then other subphases in spr3, spr2 and spr1 appear. Further softening may cause interplay between phase structures and helicoidal

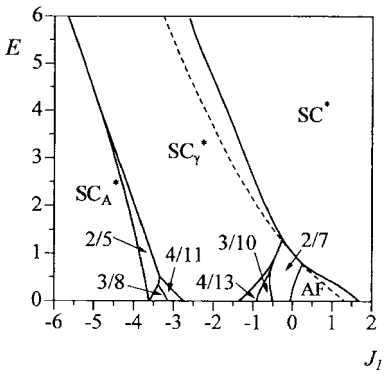

Fig. 21 E–J_1 phase diagram at $T=7.0$.[84] Some phases are indicated by their wave numbers. Solid lines show the coexisting curves and a broken line indicates the instability curve.

structures, as described in Subsection 3.5. In such extremely soft compounds, thresholdless, hysteresis-free, V-shaped switching is observed.

In this way, we can conclude that the V-shaped switching results from the frustration between antiferroelectricity and ferroelectricity.[108,109] Because of the softness, a sensitivity to substrate interfaces becomes drastic and some type of randomization is liable to occur in the molecular alignment and/or switching process.[7,8,16–18] It was reported in 1995 that the Inui mixture of **11**:**12**:**13** = 20:40:40 shows V-shaped switching as given in Fig. 22(a).[7,8] By analyzing the pretransitional phenomenon in the tristable switching, they speculated about a disordered SC_R* phase where the molecular tilting directions (the distribution of azimuthal angles) are random. The tristable switching clearly indicates that the transition between SC_A* and SC* is first order, because there exists a barrier between the molecular rotational states specified by $\psi_0{}^{AF}$ and $\psi_0{}^{F}$. The barrier may be large in some materials but small in others.[35] Let us consider what happens if the barrier diminishes or is buried in thermal fluctuations. The states characterized by any ψ_0 between $\psi_0{}^{AF}$ and $\psi_0{}^{F}$ are equally thermally excited at zero electric field; this arbitrariness of ψ_0 makes the tilting directions non-correlated because, as explained in Section 2, the tilting directions in adjacent smectic layers strongly couple with the biased directions of molecular rotation about the long axis.[31–35] Because of the extremely anisotropic tilting correlation lengths, $\xi_\perp \gg \xi_\parallel$, local in-plane spontaneous polarizations may exist at smectic layer boundaries with random orientations and variable magnitudes, as schematically illustrated in Fig. 23. Since the barrier is buried in thermal fluctuations as assumed above, the local in-plane spontaneous polarizations are thermally fluctuating. Consequently, an applied electric field induces net spontaneous polarization according to a Langevin-like equation.[7,8,18]

The difference from the ordinary Langevin equation is that we are dealing with very large effective dipole moments of variable magnitude because many molecules interact cooperatively and produce local in-plane spontaneous polarizations, and their rotation is restricted in the two-dimensional space (in the azimuthal angle).[110] Since the effective dipole moments themselves are not constant but depend on temperature, the completely aligned ferroelectric SC* state appears to be realized at a finite field. The saturation field decreases with increasing temperature as illustrated in Fig. 22(a). The induced

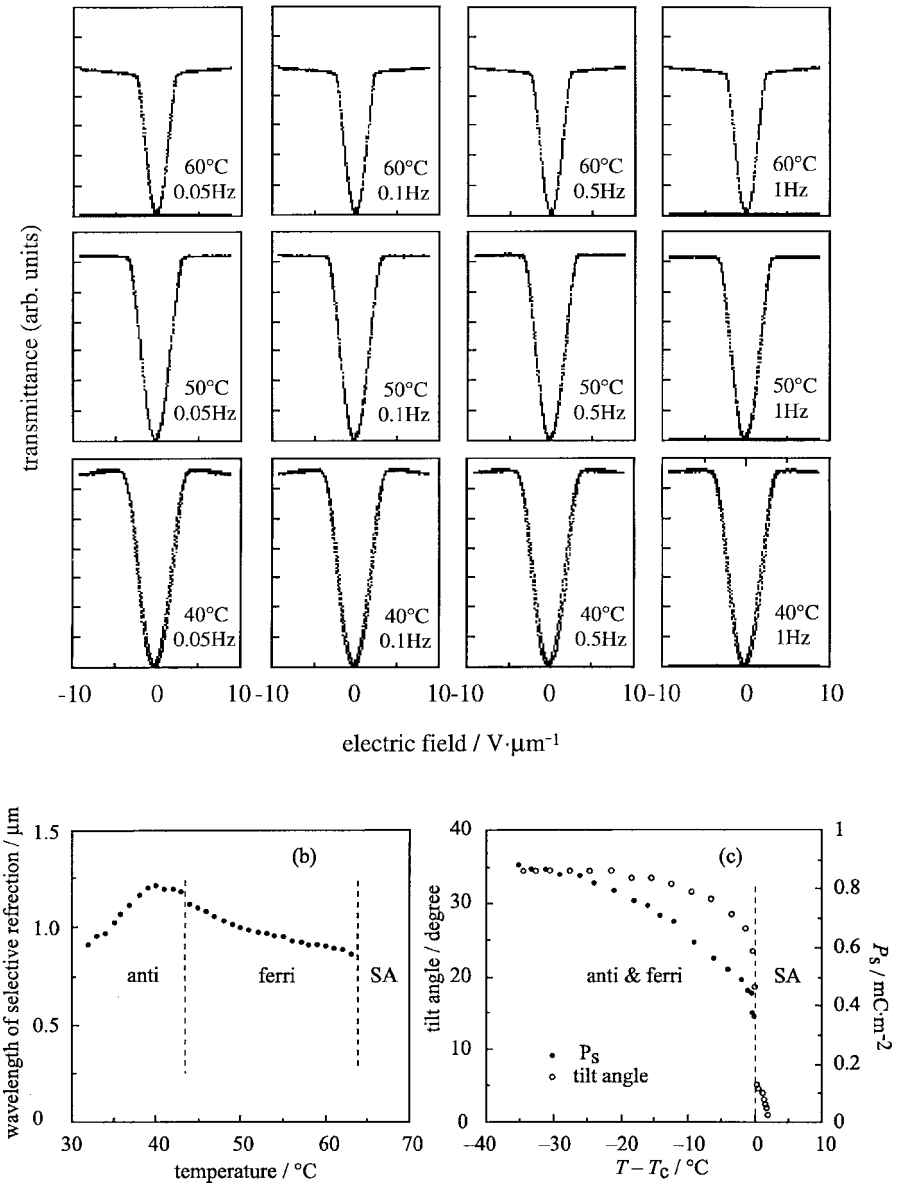

Fig. 22 Optical and electro-optical properties of the Inui mixture with **11**:**12**:**13** = 20:40:40 in Table 1. (a) The V-shaped switching observed in a homogeneous cell and (b) the temperature dependence of the peak wavelength of characteristic reflection in a free-standing film for 30° oblique incidence. For reference, the temperature dependence of spontaneous polarization measured in field-induced SC* is given in (c).[110]

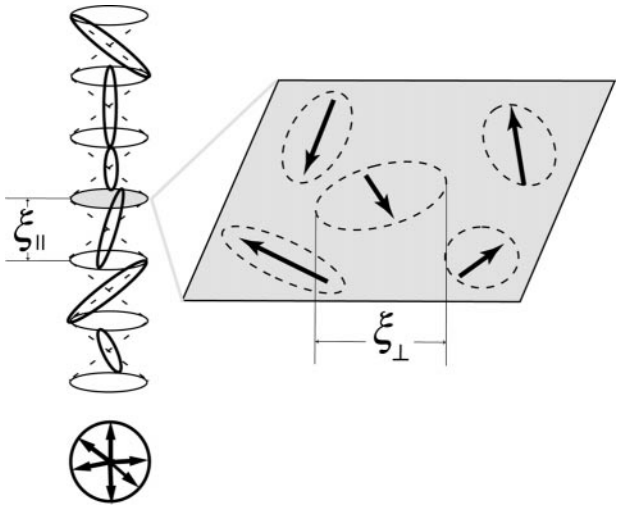

Fig. 23 A schematic illustration of the disordered phase, SC_R*, where the distribution of azimuthal angles characterizing the local C-director directions are cylindrically symmetric with extremely anisotropic correlation lengths, $\xi_\perp \gg \xi_\parallel$, and local in-plane spontaneous polarizations exist at smectic layer boundaries with random orientations and variable magnitudes.

net spontaneous polarization at a particular constant field is not inversely proportional to temperature. One may criticize that it is not appropriate to designate the switching process as a Langevin-like alignment. Moreover, the Inui mixture does not show any disordered phase when observed in a free-standing film. The electric field variation of conoscopic figures clearly indicates that it shows ferrielectric and antiferroelectric phases in the temperature region where the V-shaped switching is observed in the homogeneous cell. In fact, the characteristic reflection due to the helicoidal structure is observed in both of the phases as given in Fig. 22(b).[110] Still, we would like to emphasise the extreme softness with respect to the tilting directions and senses and the emergence of the local in-plane spontaneous polarizations at smectic layer boundaries that are fluctuating thermally. These two must play an essential role in practically usable V-shaped switching as will be explained in the following part of this section.

5.2. A disordered SC_R* phase in the bulk?

In the T–J_1 phase diagram illustrated in Subsection 4.2, SC_R* corresponds to the disordered phase above the second order critical curve.[12] The disordered phase may not be realized in an actual system, because diminished tilting correlation increases packing entropy and endangers the existence of the tilted phase itself; extremely anisotropic correlation lengths may compromise the diminished tilting correlation and an increase in packing entropy and allow the existence of SC_R*. We may be able to consider that SC_R* is almost realized as its bulk property at least in compound **11**. Apparently, a single phase emerges and it is ferrielectric. The helicoidal pitch is rather short at low and high temperatures and in-between it diverges as given in Fig. 16(a). It is tempting to speculate that J_1 varies with temperature near the minimum of the critical curve as illustrated by line (iii) in Fig. 17(b). In the temperature range where the helicoidal structure disappears, the phase may become SC_R* and the tilting correlation in adjacent smectic layers must be diminished; the helicoidal structure cannot help existing.

Since helicoidal pitch divergence results from several causes, systematic investigations need to be performed in a series of compounds where a single ferrielectric phase emerges in a wide temperature range. In three such compounds, **14**, **15** and **16**, preliminarily studied, one shows the divergence and the other two have short helicoidal pitch as shown in Fig. 16. Suppose the twisting power stays constant, less correlation may make the helicoidal pitch much shorter. Accordingly, we can conclude without contradiction that both the short pitch and its divergence result from the reduced or diminished tilting correlation in adjacent smectic layers. In Fig. 14(c), the helicoidal pitch also diverges in the ferri 2 phase. Following our speculation based on Fig. 17, any one of the antiferroelectric, ferrielectric, and ferroelectric phases may slightly enter into the disordered phase, SC_R*, and the helicoidal pitch may become infinite. Whether it abruptly jumps or gradually diverges to infinity may depend on the structure of an ordered phase under consideration. In compound **13**, we observe a jump in SC* but a gradual divergence in an antiferroelectric phase, as illustrated in Fig. 16(c). The relation between the helicoidal pitch behavior and the reduced or diminished tilting correlation in ferro-, ferri-, and antiferro-electric phases seems to be one of the interesting future problems and should be investigated by taking account of azimuthal angle fluctuations.

In this way, SC_R* in the bulk would be uniaxial, have no helicoidal structure, exhibit no threshold to an applied electric field, and continuously switch into ferroelectric SC*; a uniform uniaxial texture is expected to be observed as in SA. Since the phase is extremely soft with respect to the tilting directions, however, any additional internal and/or external forces may disturb the phase structure seriously. Actually, the in-plane correlation length $\xi_\perp$ larger than the visible wavelength may easily disturb the uniform uniaxial texture. In particular, the C-director bent caused by a linear term in the distortion free energy frequently produces hexagonal and/or rectangular patterns in the texture.[94–96] Quite recently, Rudquist *et al.*[111a,b] emphasised the charge-stabilization of a uniform SC* state (as against the disordered SC_R* state) due to the large spontaneous polarization. Anyway, no one has yet found a compound or mixture that takes SC_R* in thick free-standing films or homeotropically aligned cells. We have speculated that substrate interfaces induce some type of randomization in the molecular alignment and/or switching process, and that this randomization is responsible for the V-shaped switching.[17,18] Since it is an interface-induced phenomenon, there exist a variety of modes of the V-shaped switching. Moreover, any residual correlations may increase the varieties.

5.3. Interface-induced randomization

The two component mixtures studied in Subsection 3.5 may show V-shaped switching in homogeneous cells. Quite recently Seomun *et al.* studied the switching characteristics at various temperatures, frequencies and mixing ratios.[73,110,112,113] The homogeneous cells were prepared by sandwiching the sample between two ITO glass substrates separated by 2 μm thick polyester films; the substrates were coated with Toray SP-550 polyimide and only one of them was rubbed along one direction and sense. As originally showed by Tanaka *et al.*,[9] the **9**:**10** = 63:37 Mitsui mixture appears to give V-shaped switching at all the frequencies and temperatures investigated as illustrated in Fig. 24. In particular, even at 47 °C where an antiferroelectric phase (SC_A* or AF) stably emerges in free-standing films as seen in Fig. 13, a dc threshold does not exist and the transmittance stays nearly zero when the field is turned off. The switching differs from the apparently more ideal V-shaped one illustrated in Fig. 22 in two respects: (1) steps (arrows 1 and 2) are observed at low temperatures, rather distinctly before complete switching to ferroelectric SC* but indistinctly after starting to decrease down to the minimum; and (2) it shows some hysteresis and looks W-shaped near the minimum (arrow 3). Note that, as is clear by comparing Fig. 13(a) and (b), only one liquid crystal phase other than SA is distinguished in homogeneous cells, while five tilted phases are observed in free-standing films. Substrate interfaces destroy the phase structures, although some residual tilting

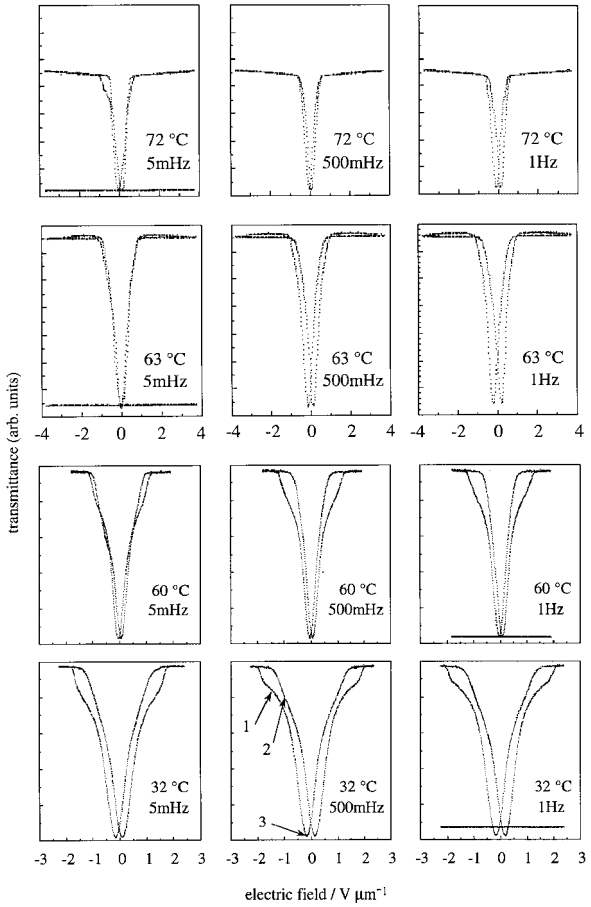

Fig. 24 The V-shaped switching observed in the Mitsui mixture of **9**:**10** = 63:37 in Table 1.[110]

correlations stabilizing ferrielectric phases may cause the steps near the critical field.

In a mixture with **9**:**10** = 70:30, the stable state at 52 °C is an antiferroelectric phase (SC_A* or AF) not only in a free-standing film but also in a homogeneous cell. The threshold is clearly seen in the first run of the electro-optic switching, although some thresholdless switching is achieved dynamically, as shown in Fig. 25. In the **9**:**10** = 63:37 mixture, however, the stable state at 52 °C is not an antiferroelectric phase (SC_A* or AF) in a homogeneous cell because no threshold is observed as mentioned above, although it is in a free-standing film. Destruction of the subphase structures by substrate interfaces is also seen in the temperature dependence of dielectric constants given in Fig. 26. In a mixture with **9**:**10** = 66:34, the existence of the Goldstone mode distinguishes ferroelectric SC* from antiferroelectric SC_A* or AF. In the mixture with **9**:**10** = 63:37, however, the relative permittivity becomes

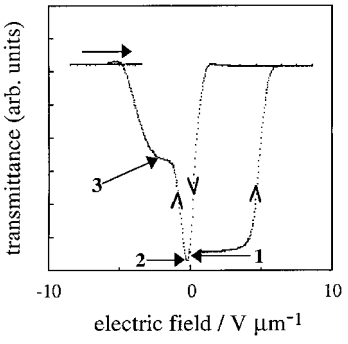

Fig. 25 The electro-optic switching in a mixture with **9**:**10** = 70:30 in Table 1.[73,110] The dc threshold appears in the first run and then some thresholdless switching is achieved dynamically.

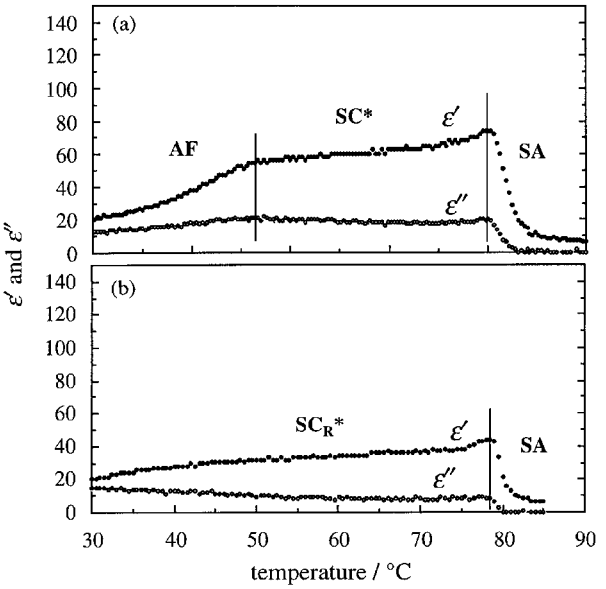

Fig. 26 The temperature dependence of relative permittivities in (a) a mixture with **9**:**10** = 66:34 and (b) a mixture with **9**:**10** = 63:37.[73,110]

smaller, the phase transition disappears and a single phase or state prevails. The state is neither ferroelectric nor antiferroelectric; no helicoidal structure exists, either. Still, it becomes very dark at the tip of the V where the applied electric field is zero. Considering the softness with respect to the tilting directions, explained in Subsections 3.5 and 5.1, the only alternative left is to consider that substrate interfaces introduce some type of randomization in the tilting directions. The intrinsic randomization, if any, is the one depicted in Fig. 23. Substrate interfaces deform this in various ways and the azimuthal angle distribution may not be cylindrically symmetric around the smectic layer normal as originally speculated.[8] When molecules are constrained to become parallel to the interfaces, they tilt to the right or to the left randomly from layer to layer; this situation may also be described as a disordered ferrielectric state with stripe domains narrower than the visible light wavelength.[16] When a rubbing direction exerts strong anchoring on molecules, on the other hand, the similar Ising type randomization is realized perpendicularly to the substrate interfaces;†† the chevron structure may complicate the actual molecular alignments.

Considerably polar interfaces are characteristic in the sense that not randomization but ferroelectric order is induced at least on the interfaces. In fact, so-called twisted states were formed in the **9**:**10** = 63:37 mixture.[110,113] It was aligned homogeneously by the temperature gradient method after being sandwiched between ITO glass substrates using a polyester film spacer. The cell thickness was about 2.6 μm. Fig. 27 shows optical micrographs in the virgin cell before applying an electric field. The region (a-1) has electrodes on both surfaces, while the regions (a-2) and (a-3) have an electrode on either the top or the bottom surface. The extinction is along the layer normal in the region (a-1), while the regions (a-2) and (a-3) become dark by rotating the layer normal by 14 and −13°. The tilt angle obtained by applying a high

††If the antiferroelectric phase exists as considered by Pauwels *et al.*,[114,115] the threshold should be observed. If the ferroelectric order remains to exist as reported quite recently by Takezoe *et al.*[116] and Park *et al.*,[117] on the other hand, the Goldstone mode should appear more clearly. Actually, both of them were observed in free-standing films, respectively, in the corresponding phase and even in the homogeneous cells of **9**:**10** = 30:70 and 66:34. Consequently, the smaller relative permittivity and the disappearance of the phase transition inevitably require Ising type randomization even in the strong anchoring along the rubbing direction.

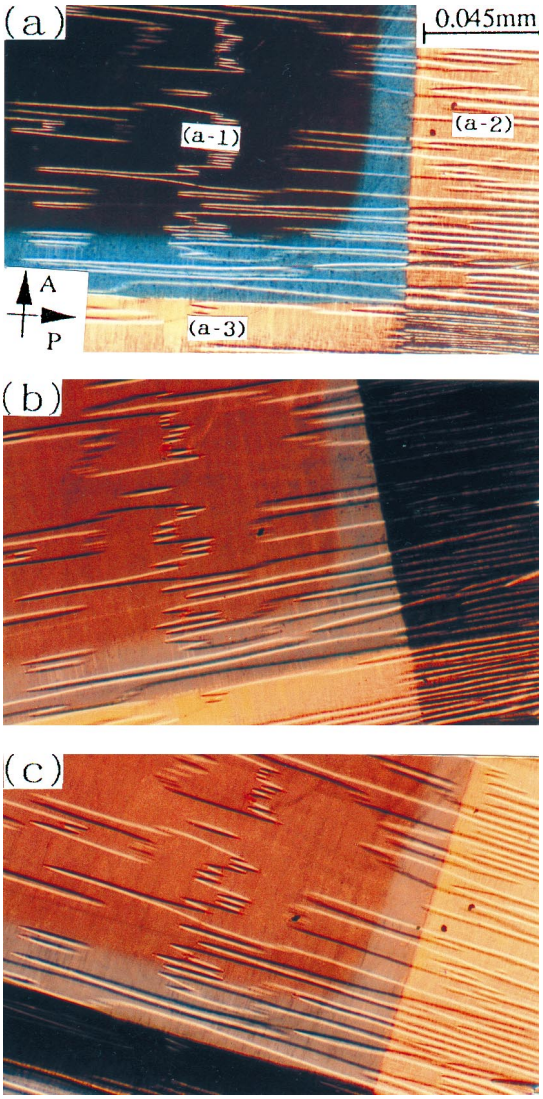

Fig. 27 Optical micrographs of a 2.6 μm thick Mitsui mixture cell aligned by the temperature gradient method after being sandwiched between ITO-coated glass substrate plates using a polyester film spacer.[110,113]

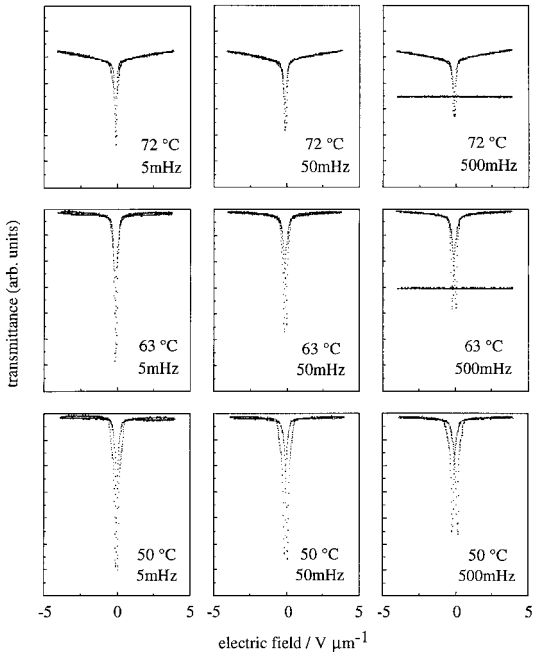

Fig. 28 The V-shaped switching observed in the same cell as the one used in Fig. 27.[110,113]

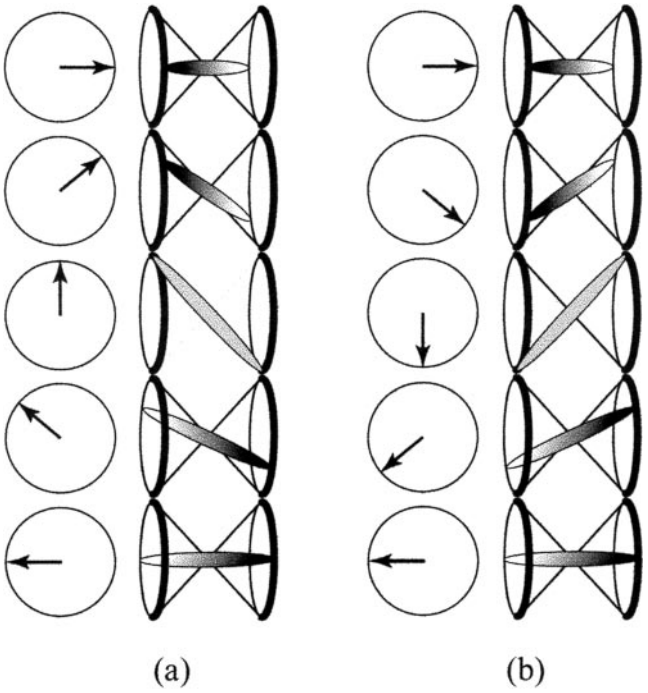

Fig. 29 Two kinds of twisted states, the random coexistence of which may ensure the low transmittance at the tip of the V in Fig. 24.[118]

enough electric field is 28°. Fig. 27 indicates that the twisted state is realized in the region (a-1), where molecules tilt in the opposite senses on the top and bottom surfaces. Fig. 28 shows that the switching is similar to the V-shaped one given in Fig. 24. Two differences are: (1) the transmittance at the tip of the V was fairly high, and (2) during the switching, somewhat thick stripe domains perpendicular to the smectic layer normal were observed with a polarizing optical microscope. The fairly high transmittance results partly from the twisted state and partly from the thick stripe domains. The appearance of the stripe domains indicates a reduced interlayer tilting correlation. If the domains are thinner than the visible light wavelength, the texture may become much more uniform. Although detailed studies have not yet been carried out, randomization is considered to occur in the two kinds of twisted states illustrated in Fig. 29[118] These two may coexist randomly from layer to layer; the random coexistence ensures the low transmittance at the tip of the V.

5.4. Extreme uniformity in V-shaped switching

One of the characteristic features of V-shaped switching is that whole changes in transmittance increase and decrease sometimes proceed quite uniformly, without any accompanying boundary movement. We will show an example[17,35,110] in the following. The sample used is compound **12**, which is a component of the Inui mixture described in Subsection 5.1. Fig. 30 shows the temperature variation of the spontaneous polarization measured in electric field induced SC* using a homogeneous cell. The temperature dependence of the peak wavelength of characteristic reflection in a free-standing film for 30° oblique incidence is given in Fig. 16(b). The electric field dependence of conoscopic figures indicates that the higher temperature phase is ferrielectric and the lower temperature one is antiferroelectric. Since no peak exists in the shorter wavelength region, the observed peak is a normal characteristic reflection (a half-pitch band). We expect to observe a full-pitch band in the longer-wavelength region in the ferrielectric phase; the observation was not possible because

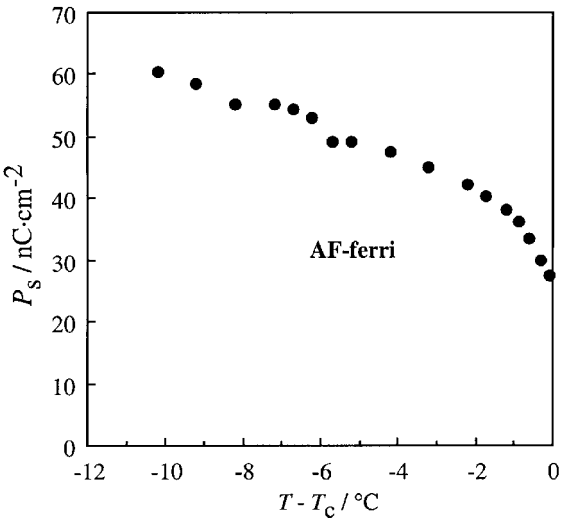

Fig. 30 The temperature dependence of the spontaneous polarization measured in field-induced SC*.[110]

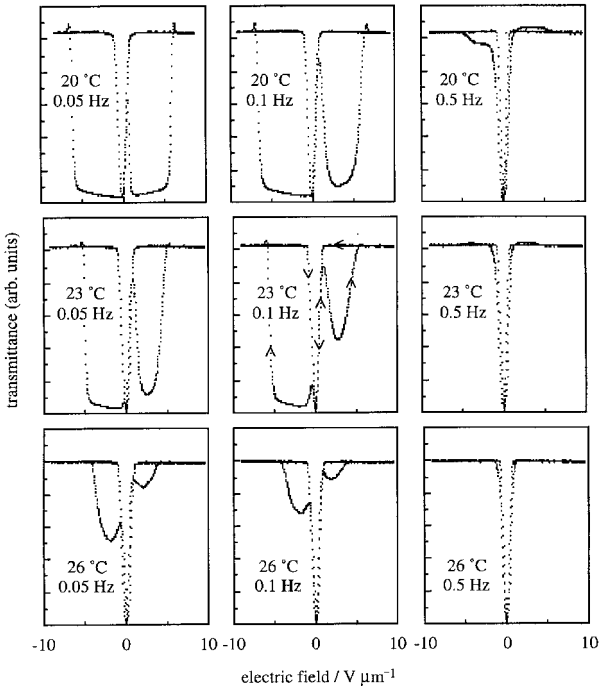

Fig. 31 The evolution of switching characteristics observed in a homogeneous cell prepared by the polyimide rubbing method of compound **12**.[17,110]

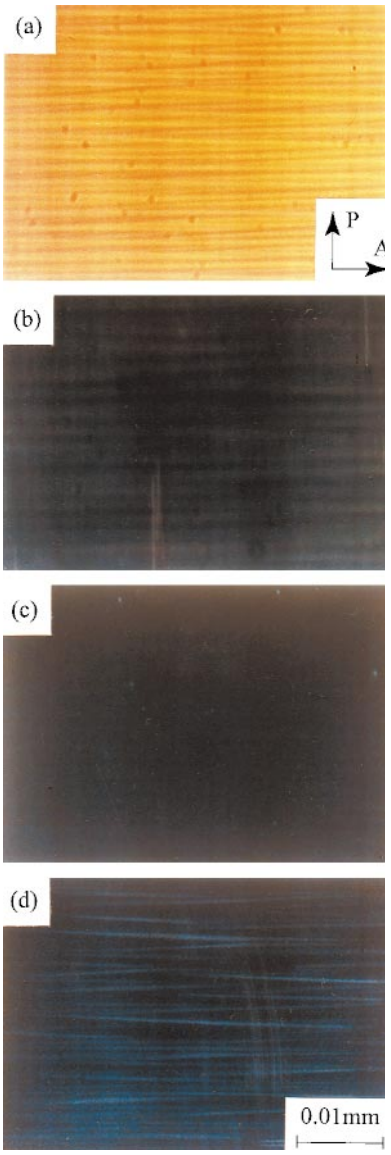

Fig. 32 A series of micrographs of the same cell as used in Fig. 31 taken at 29 °C in (a) the ferroelectric bright state, (b) a gray state midway, and (c) the dark state at the tip of the V. For comparison, a micrograph taken without applying any field is shown in (d).[17,110]

of the limitation of the wavelength range in the spectrophotometer used. DSC revealed that the antiferroelectric phase directly changes into a crystalline phase at about −31 °C. We did not identify whether the antiferroelectric phase is SC_A* ($q=1/2$) or AF ($q=1/4$). The longer pitch in the antiferroelectric phase compared with that in the ferrielectric phase may suggest that it is not SC_A* but AF. Empirically, the helicoidal handedness of SC_A* is generally opposite to that of SC* and the helicoidal pitch of any subphase is generally longer than that of SC_A*. In any case, it is a typical phase sequence; in particular, the antiferroelectric phase does not become thresholdless in free-standing films.

Fig. 31 illustrates the electro-optic responses observed in a homogeneous cell prepared by the polyimide (Toray SP-510) rubbing method as described in Subsection 5.3. At 50 mHz and 20 °C, the transmittance *vs.* electric field (*Tr–E*) curve shows almost typical tristable switching characteristics in the antiferroelectric phase, although the curve is slightly asymmetric and the positive side exhibits some anomalous behavior. As the frequency and/or temperature increases, this anomaly becomes conspicuous, appears also on the negative field side, and evolves into V-shaped switching. At 29 °C, nearly ideal V-shaped switching is observed as shown in Fig. 31. During the V-shaped switching, the apparent tilt angle continuously rotates from zero to the tilt angle $\theta \approx 35^\circ$ in ferroelectric SC*, which is attained at the saturation field E_5. If we rotate the polarizer axis by $\pm\omega$ from the smectic layer normal, keeping the analyzer crossed, the transmittance now becomes zero at $\pm E(\omega) \neq 0$. Here ω is smaller than θ and $E(\omega)$ is lower than E_c. The transmittance at the tip of the V is lower than the lowest one in the tristable switching. This difference is also seen in textures.

Fig. 32(a)–32(c) are micrographs taken during the switching process of transmittance decrease with the application of a triangular waveform electric field, and Fig. 32(d) is the texture observed without applying any field. There is a difference between Fig. 32(c) and 32(d), both of which were obtained at zero field. The texture at the tip of the V appears to be darker and more uniform than the one taken without applying any field. In Fig. 32(d), there remains a kind of stripe defects

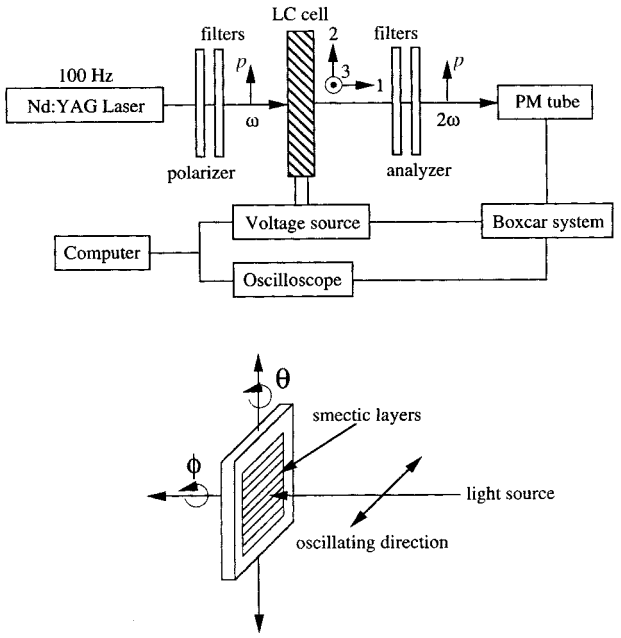

Fig. 33 Schematic drawing of the experimental set-up for SHG from a homeotropically aligned liquid crystal cell.[123]

parallel to the smectic layer normal. Although the stripe defects are more clearly seen in the ferroelectric bright state given in Fig. 32(a), the V-shaped switching itself proceeds quite uniformly without any accompanying boundary movement. In the tristable switching, on the other hand, the abrupt increase at the threshold field always accompanied the characteristic domain boundary movement.[119–121] The movement was always observed, even when the tristable switching occurred atypically as in the case given in Fig. 31.

What molecular arrangement is realized at the tip of the V? Since no domain boundary movement is observed during the steep, almost linear decrease from ferroelectric SC* to zero, a conceivable simple process is either of the extremes: the highly collective azimuthal angle rotation of the long molecular axes or the sufficiently random one. Since the tilting correlation between adjacent layers must be reduced considerably, the random process is probable. The extreme uniformity, in particular, the disappearance of the stripe defects parallel to the smectic layer normal, strongly supports the random process.‡‡ Let us consider the randomization process in more detail. When the interaction between the sample and the substrate interfaces used is kept weak, *i.e.*, just strong enough to generate the bookshelf structure in SA, the interfaces do not macroscopically constrain the tilting directions (specified by the azimuthal angle) in the SC*-like phase. In fact, such interfaces are used in deformed helix ferroelectric (DHF)-LCDs.[122] By taking account of the fact that the interfaces themselves consist of polymer molecules, however, liquid crystalline molecules are forced to tilt randomly on the microscopic scale, not only in the right and left but also in the azimuthal angle distribution. This microscopic constraint§§ comes to play an important role when the tilting correlation in adjacent layers is reduced considerably. The substrate interfaces may induce randomization, breaking the residual intrinsic tilting correlation from layer to layer.[17,18] In a single smectic layer, however, the tilting correlation must still be so high that the local in-plane spontaneous polarizations emerge at smectic layer boundaries.

5.5. Several modes of V-shaped switching and a practically usable one

The V-shaped switching we are studying here is considered to be caused by frustration between antiferroelectricity and ferroelectricity. The frustration is one of the key points we have made above in this Article. Quite recently, Rudquist *et al.*,[111a,b] Takezoe *et al.*,[116] and Park *et al.*[117] studied the Inui mixture, **11**:**12**:**13** = 20:40:40. They concluded that the charge stabilization and/or the highly collective azimuthal angle rotation of the long molecular axes is essential in the V-shaped switching. As explained in Subsection 5.3, the charge stabilized ferroelectric SC* state, aligned along the rubbing direction or twisted, may be realized by preparing the cell in the manner they described, since the material is very soft with respect to the tilting direction and has large spontaneous polarization. The existence of such charge-stabilized states is not in contradiction to our notion about the frustration. Regarding the highly collective rotation, it may also be possible if the charge stabilization is really effective. An open question is: to what extent the charge stabilization can realize the uniformity of the V-shaped switching stably.¶¶ In an appropriately prepared Inui mixture cell that shows almost ideal V-shaped switching, however, we still suspect randomization, *e.g.* the one described in 5.3, to play an important role in the molecular alignment and/or switching process. A conceivable difficulty in the collective rotation is that the state at the tip of the V is not unique; there exist two states, one formed from a ferroelectric state induced by a positive electric field and the other formed from another ferroelectric state at a negative electric field. Such a duality may cause the switching stability to deteriorate.

Anyway, there exist a variety of modes of V-shaped switching in such an extremely soft SC* like phase. For the practically usable one, we believe, some type of randomization is necessary. In particular, the two dimensional (ideally, cylindrically symmetric) azimuthal angle distribution of local in-plane directors around the smectic layer normal is most attractive. Such a randomized state at the tip of the V is thermodynamically unique under a given condition imposed by interfaces. It stays stable even when the smectic layer structure, such as chevron, changes with temperature. Consequently, remarkably uniform switching is certain to occur with a very high contrast ratio in a wide temperature range. The V-shaped switching (the dielectric property) that is related to some type of randomization in the extremely soft SC* like phase had better be called 'frustoelectricity' or 'frustrated electricity' although it was initially designated as 'thresholdless antiferroelectricity'.‖‖ It is caused by the frustration between ferro- and antiferro-electricity. To commercialize AM(TFT)-LCDs using frustoelectricity (FR-AM-LCDs), it is important to ensure appropriate randomization. Here the highly sophisti-

‡‡One may still adhere to the collective azimuthal angle rotation of the long molecular axes as Rudquist *et al.*,[111a,b] Takezoe *et al.*[116] and Park *et al.*[117] actually did quite recently. However, we could not devise an explanation of how the collective molecular rotation makes the stripe defects apparently disappear.

§§We have experienced this microscopic constraint to such an extent that we could not grow an SA monodomain from the edge of a polyester film spacer by the temperature gradient method[118] using ITO glass substrates coated with polyimide (Toray SP-550). Polyimide moieties strongly constrain liquid crystal molecules in various directions from place to place. These constraints make it difficult for the molecules as a whole to become parallel to the polyester spacer edge.

¶¶We wish to emphasize one point. They just simulated, and did not prove experimentally, that the collective rotation realized the extremely uniform switching. The switching itself may still be characterized by some random processes.

‖‖The antiferroelectricity results from the characteristic bent shape of constituent molecules. Emphasizing the antiferroelectric interaction, all the compounds and mixtures that show any of the subphases including SC_A* are designated as antiferroelectric liquid crystal materials. In some such materials, V-shaped switching was observed and hence it was thought quite natural to call the materials 'thresholdless AFLCs' from an application point of view. It was inappropriate, however, to designate the dielectric property (the V-shaped switching) as 'thresholdless antiferroelectricity', because there exists no antiferroelectric order.[108]

Table 2 Mixtures developed by Mitsui Chemicals Inc.[129]

(I-1) 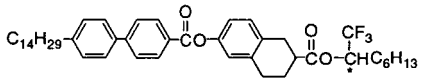

(I-2) 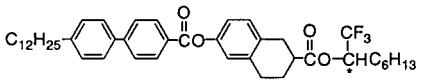

(I-3) 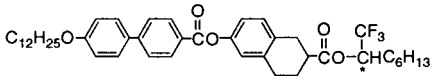

(I-4) 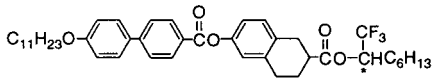

(I-5) 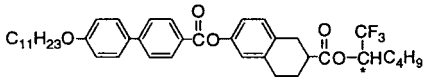

(I-6) 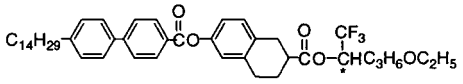

(I-7) 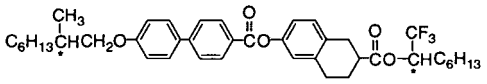

(I-8) 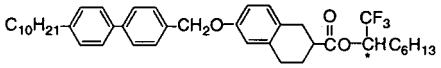

(I-9) 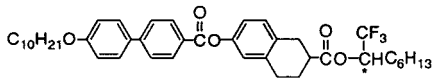

(I-10) 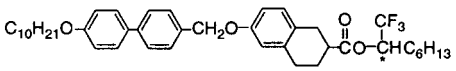

(I-11) 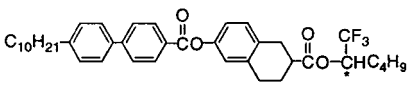

(I-12) 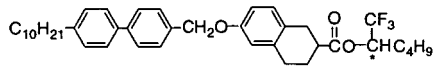

(I-13) 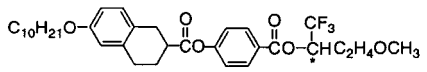

(I-14) 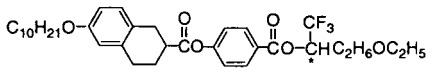

(I-15) 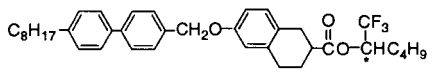

(I-16) 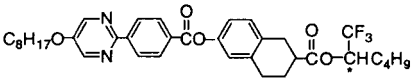

(I-17) 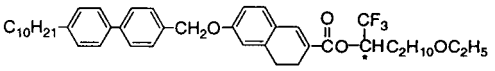

(I-18) 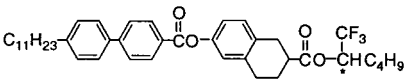

(I-19) 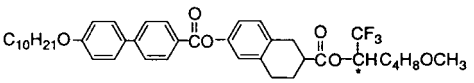

(I-20) 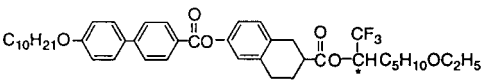

(I-21) 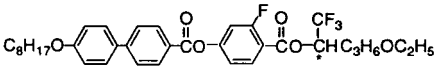

(I-22) 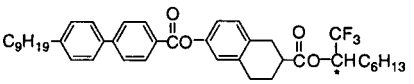

(I-23) 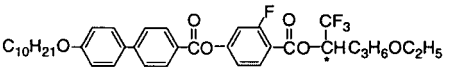

(I-24) 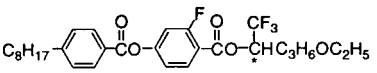

(I-25) 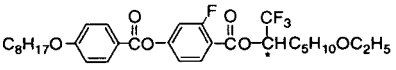

(I-26) 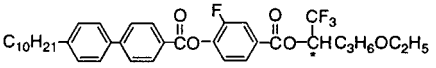

(II-1) 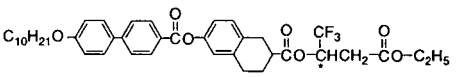

(II-2) 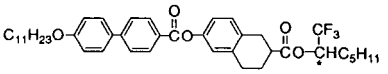

(II-3) 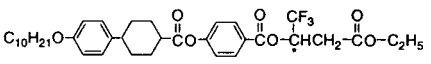

(II-4) 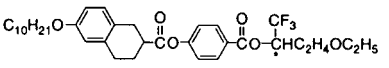

(II-5) 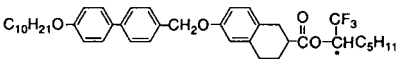

Mixture no.	I-1 Weight %	I-2	I-3	I-4	I-5	I-6	I-7	I-8	I-9	I-10	II-1	II-2	II-3	T_{max}(anti)/ °C	T_{max}(ferro)/ °C	T(iso)/ °C
E1	10.3	10.3	41.2	10.3							27.9			78		100
E2	10	10	40	10							30			77		99
E3	9.44	9.44	37.7	9.44							34			75		96
E4	8.88	8.88	35.4	8.88							38			73		93
E5	8.6	8.6	34.3	8.6							40			73		93
E6	7.1	7.1	28.6	7.1							50			68		87
CE1	5.7	5.7	22.9	5.7							60				63	79
CE2	14.3	14.3	57.1	14.2							0			86		113
E7					48	47					5			80	105	132
E8							20	20				60		82		107
E9	76							5			19			51	56	87
E10	10			10					10	40	30			68		92
E11	10	10	40						10		20		10	68		98
E12	10	10	40						10				30	78	91	118

Table 2 (*Continued*).

Mixture no.	I-2	I-6	I-11	I-12	I-13	I-14	I-15	I-16	I-17	II-4	II-5			T_{max}(anti)/°C	T_{max}(ferro)/°C	T(iso)/°C
	Weight %															
E13	80	20												82		102
E14	90		10											87		108
E15		20		80										75		85
E16				80	20									59		65
E17				80						20				56		58
E18				80		20								53		55
E19				80				20						53		55
E20				34			14	30		10	12			68		84
E21				64		20			16					54		56
E22				56		20			24					43		44
E23				44		19	16				20			58		64
Mixture no.	I-3	I-6	I-7	I-11	I-18	I-19	I-20	I-21	I-22	I-23	I-24	I-25	I-26	T_{max}(anti)/°C	T_{max}(ferro)/°C	T(iso)/°C
	Weight %															
E24			20		80									85		109
E25				50		50								86		114
E26						50	50							88		117
E27							50	50						99		117
E28						40		60						104		119
E29	20							80						105		110
E30					20			80						103		111
E31								50	50					97		112
E32		50						50						90		104
E33								20		80				50		57
E34								20			80			98		100
E35										50		50		61		64
E36										50			50	57		69

cated technology is to balance ferro- and antiferro-electricity in liquid crystal materials and to develop attractive polyimide aligning films so that the frustration manifests itself to its fullest extent.

For checking the randomization, it is useful to analyze in detail not only the ordinary switching process but also the second harmonic generation (SHG) together with its coherence characteristics. Because of the existence of local in-plane spontaneous polarizations at smectic layer boundaries, as schematically illustrated in Fig. 23, we will observe a reasonably strong SHG signal in the experimental geometry shown in Fig. 33. Because of their random orientations and variable magnitudes, the SHG signals should not be coherent. If the signal is partially coherent as actually observed by Seomun *et al.*,[123] molecular alignments are not completely random and some order remains in existence at the tip of the V. This causes the stability of the V-shaped switching to deteriorate. When a rubbing direction exerts strong anchoring on molecules, as pointed out in Subsection 5.3, the azimuthal angle distribution of in-plane directors is not considered cylindrical. Still, a considerably strong, incoherent SHG signal may be observed. Consequently, it is necessary to check the azimuthal angle distribution by polarized IR and/or Raman spectroscopy. In this way, the V-shaped switching critically depends on the cell fabrication method, *i.e.* the choice of aligning polyimide and insulating materials together with their thickness. We would like to perform the SHG and spectroscopic measurements using the same cell in which the practically usable V-shaped switching has been confirmed to occur stably. We are in the process of establishing the method for evaluating the molecular alignments at the tip of the V.

6. Application to liquid crystal displays

The growing demand for monitor applications of liquid crystal displays (LCDs) has improved viewing angles to an acceptable level of more than 70° by active matrix (AM) electrodes, *i.e.* thin film transistors (TFTs).[124–127] In the multimedia environment, moving pictures are becoming more and more common, and consequently monitors are required to have sufficiently

Table 3 Compounds developed by Mitsubishi Gas Chemical Company, Inc.[16,130–134]

3a
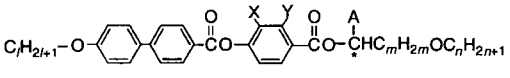

3b
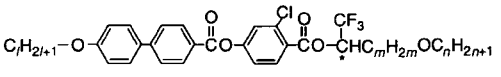

3c
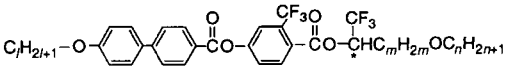

3d
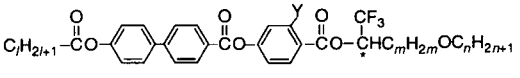

3e-1
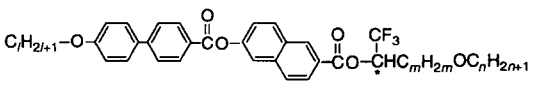

3e-2
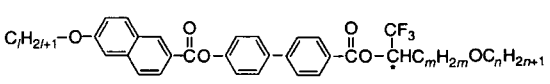

3e-3
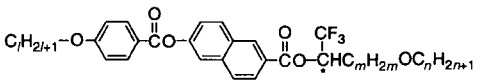

Table 3a

Compound	no.	*l*	X	Y	A	*m*	*n*	Phase sequences (°C)
15	E35	8		F	CF_3	2	2	cry (58) ferri (104) SA (108) iso
	E36	9		F	CF_3	2	2	cry (73) ferri (104) SA (115) iso
	E37	9	F		CF_3	2	2	cry (50) ferri (73) SA (98) iso
	CE1	7		F	CF_3	3	2	cry (62) SC* (113) SA (116)iso
	CE2	8		F	CF_3	3	2	cry (56) SC* (108) SX (110) iso
4-1C	E1	9		F	CF_3	3	2	cry (34) ferri (101) SA (103) iso
	E2	10		F	CF_3	3	2	cry (33) ferri (98) SA (99) iso
	E3	11		F	CF_3	3	2	cry (35) ferri (95) SA (96) iso
	E4	12		F	CF_3	3	2	cry (41) ferri (92) SA (94) iso
	E5	9		F	CF_3	3	3	cry (< −10) ferri (99) SA (102) iso
	E6	9		F	CF_3	3	4	cry (< −10) ferri (92) SA (95) iso
16	E7	9			CF_3	3	2	cry (61) ferri (108) SA (115) iso
	E8	9			CF_3	3	3	cry (56) ferri (104) SA (110) iso
	E9	9			CF_3	3	4	cry (50) ferri (97) SA (105) iso
	E10	9	F		CF_3	3	2	cry (71) ferri (81) SA (99) iso
	E11	9	F		CF_3	3	3	cry (66) ferri (76) SA (94) iso
	E12	9	F		CF_3	3	4	cry (60) ferri (69) SA (89) iso
	E14	6		F	CF_3	4	2	cry (46) ferri (107) SA (115) iso
	E15	7		F	CF_3	4	2	cry (51) ferri (98) SX (103) iso
4-1A	E16	8		F	CF_3	4	2	cry (46) ferri (95) SA (98) iso
4-1B	E13	9		F	CF_3	4	2	cry (< −10) ferri (89) SA (91) iso
	E17	10		F	CF_3	4	2	cry (< −10) ferri (85) SX (86) iso
11	E18	11		F	CF_3	4	2	cry (29) ferri (82) SA (84) iso
	E19	12		F	CF_3	4	2	cry (40) ferri (82) SX (83) iso
	CE3	8		F	CF_3	4	3	cry (38) anti (96) SC* (97) SA (98) iso
	E20	9		F	CF_3	4	3	cry (< −10) ferri (84) SX (88) iso
	CE4	11		F	CF_3	4	3	cry (25) anti (79) ferri (83) iso
	E21	9		F	CF_3	4	4	cry (< −10) ferri (79) SX (84) iso
	CE6	8			CF_3	4	1	cry (73) anti (106) SA (114) iso
	CE5	6			CF_3	4	2	cry (98) anti (104) SA (117) iso
	E23	7			CF_3	4	2	cry (93) ferri (104) SX (118) iso
	E24	8			CF_3	4	2	cry (57) ferri (101) SA (111) iso
14	E22	9			CF_3	4	2	cry (−30) ferri (95) SA (103) iso
	E25	10			CF_3	4	2	cry (48) ferri (92) SA (99) iso
	E26	11			CF_3	4	2	cry (28) ferri (86) SX (93) iso
	E27	12			CF_3	4	2	cry (54) ferri (85) SX (90) iso
	E28	9			CF_3	4	3	cry (41) ferri (88) SA (96) iso
	E29	9			CF_3	4	4	cry (37) ferri (83) SA (95) iso
	CE8	9	F		CF_3	4	1	cry (55) anti (71) SA (89) iso
	CE7	7	F		CF_3	4	2	cry (84) SA (103) iso
	E31	8	F		CF_3	4	2	cry (62) ferri (73) SA (97) iso
	E30	9	F		CF_3	4	2	cry (47) ferri (66) SA (85) iso
	E32	12	F		CF_3	4	2	cry (40) ferri (61) SA (73) iso
	E33	9	F		CF_3	4	3	cry (41) ferri (60) SA (82) iso
	E34	9	F		CF_3	4	4	cry (40) ferri (55) SA (77) iso
	E38	8		F	C_2F_5	4	2	cry (30) ferri (70) iso
	E39	10		F	C_2F_5	4	2	cry (20) ferri (57) iso
	E40	11		F	C_2F_5	4	2	cry (34) ferri (51) iso
	E41	9		F	CF_3	5	1	cry (< −20) ferri (83) iso
	E42	8			CF_3	5	1	cry (79) ferri (100) SX (105) iso
	E43	9			CF_3	5	1	cry (53) ferri (92) SX (96) iso
	CE9	6		F	CF_3	5	2	cry (55) anti (102) SA (105) iso
	CE10	8		F	CF_3	5	2	cry (40) anti (89) iso
	CE11	9		F	CF_3	5	2	cry (?) anti (82) SC* (83) iso
	CE12	10		F	CF_3	5	2	cry (26) anti (80) iso
	CE13	14		F	CF_3	5	2	cry (49) anti (70) iso
	CE14	9			CF_3	5	2	cry (33) anti (83) SC* (88) SA (94) iso
13	CE15	11			CF_3	5	2	cry (?) anti (73) SC* (83) SA (?) iso
	E44	9			CF_3	5	3	cry (54) ferri (85) SX (90) iso

Table 3b

Compound	no.	*l*	X	Y	A	*m*	*n*	Phase sequences (°C)
	E1	9		Cl	CF_3	2	2	cry (< −60) ferri (77) SA (80) iso
	E2	9		Cl	CF_3	3	2	cry (< −60) ferri (84) SA (87) iso
	E3	9		Cl	CF_3	4	2	cry (< −60) ferri (68) SA (70) iso
	E4	9		Cl	CF_3	5	1	cry (< −60) ferri (62) iso
	CE1	8		Cl	CF_3	5	2	cry (< −20) anti (68) SC* (69) iso
	CE2	9		Cl	CF_3	5	2	cry (< −30) anti (53) SC* (63) iso
	E5	9		Cl	CF_3	5	3	cry (< −23) ferri (60) iso
	CE3	8		Cl	CF_3	7	2	cry (< −50) anti (57) iso

Table 3c

Compound	no.	*l*	X	Y	A	*m*	*n*	Phase sequences (°C)
	E1	9		CF_3	CF_3	2	2	cry (34) ferri (48) iso
	E2	9		CF_3	CF_3	3	2	cry (31) ferri (55) iso
	E3	9		CF_3	CF_3	4	2	cry (4) ferri (40) iso

Table 3d

Compound	no.	*l*	X	Y	A	*m*	*n*	Phase sequences (°C)
	E1	9		F	CF_3	3	2	cry (48) ferri (101) SA (105) iso

Table 3e

Compound	no.	*l*	X	Y	A	*m*	*n*	Phase sequences (°C)
3e-1	CE1	9			CF_3	5	2	cry (68) anti (92) ferro (121) SA (142) iso
3e-2	CE2	8			CF_3	5	2	cry (52) anti (78) SX (79) SA (134) iso
3e-2	E1	9			CF_3	5	2	cry (54) ferri (87) SA (126) iso
3e-3	CE2	12			CF_3	5	2	cry (−4) anti (6) iso

Size	5.5 inch diagonal
Resolution	QXGA (240 x 320 x 3)
Scanning time per line	60 ms
Refresh frequnecy	30 Hz
Driving voltage	2.5 V
Contrast ratio	> 300

Fig. 34 A picture shown on a 5.5 inch, full-color, video rate LCD which Casio recently prototyped and exhibited at the Electronics Show 97.[27] (By courtesy of Casio Computer Co., Ltd.)

Size	15 inch diagonal
Resolution	XGA (768 x 1024 x 3)
Contrast ratio	> 100
Gray level response time	< 50 ms
Gray scale	64 levels (6 bit)
Driving scheme	Qusi-dc driving
Viewing angle	> 70 deg.
Driving voltage	5 V

Fig. 35 A picture shown on a 15 inch, full-color, video rate LCD which Toshiba recently prototyped and exhibited at the 1997 Toshiba Electronics Show.[141,142] (By courtesy of Toshiba Corp.)

fast response times not only between black and white levels but also between any gray levels. However, no AM-LCDs so far developed using nematic liquid crystals have realized fast enough response times. The V-shaped switching due to frustoelectricity is promising for realizing attractive AM-LCDs.[128] Since the optical axis rotates between 0 and $\pm\theta^\circ$ continuously in a plane parallel to the substrate glass plates, the V-shaped switching is not only a kind of in-plane switching but also symmetric with respect to the smectic layer normal. Consequently, the viewing angle is very wide. Randomization together with thermal fluctuation of local in-plane C-directors ensures uniformity free from hysteresis, *i.e.* high contrast ratio and ideal analog gray scale, as demonstrated in Fig. 22 and 32. Because of the emergence of local in-plane spontaneous polarizations at smectic layer boundaries, linear coupling with an applied electric field makes the response speed very fast. In fact, Chen *et al.*[128] reported that a 2 μm thick test cell of a frustoelectric smectic mixture ($P_s = 0.92\ mC\ m^{-2}$ ($92\ nC\ cm^{-2}$)) shows the response time τ_{90} in the range of 0.1–1 ms for the 2 (black and white) –32 gray scale displaying at a maximum applied voltage of 6 V.

As an inevitable consequence, frustoelectric liquid crystals (FR-LCs) and polyimide aligning materials have been developed actively. Although little information about the aligning films have been disclosed, several FR-LC materials have been reported in Japanese Patent Gazettes. As access to these publications written in Japanese may not be easy for non-Japanese scientists and engineers in the liquid crystal community, and as these sources contain valuable information, we will try to summarize the FR-LC materials. Table 2 summarizes 36 examples (E1–E36) of mixtures together with two comparative ones (CE1 and CE2) developed by Mitsui Chemicals Inc.[129] They listed two groups of compounds, **I-1**–**I-26** and **II-1**–**II-5**, and suggested mixing some of them to produce materials showing V-shaped switching as given in Tables 2-1, 2-2 and 2-3. Their basic idea is the same as described in

Subsection 5.3 to balance antiferroelectricity and ferroelectricity, although they did not use the term 'frustration'. They seemed to consider that group I and II compounds are antiferroelectric and ferroelectric, respectively. In fact, compounds **I-3** and **II-3** in Table 2 are the same as compounds **9** and **10** in Table 1. As is seen Fig. 13, this consideration is correct to some extent. Since they did not observe the electric field dependence of conoscopic figures using free-standing films, the phase assignments are not clear. In particular, they did not mention the existence of ferrielectric phases. They just

Table 4 Mixtures developed by Mitsubishi Gas Chemical Company, Inc. They emphasise lower saturation field, E_s, and faster response speed, τ_{90}, in mixtures **4a**/**4b**–E1–E23,[135] **4c**–E1–E4,[136] and **4d**–E1;[140] better alignment and hence lower transmission at the tip of the V, *Tr*, in mixtures **4e**–E1,[137] **4f**–E1,[138] and **4g**–E1.[139]

4a

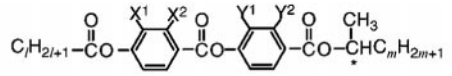

4b

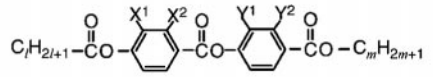

4c

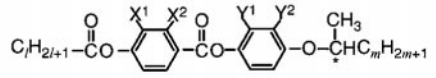

4d

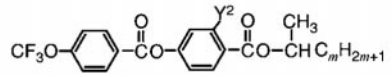

4e

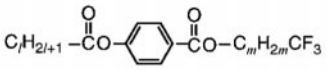

4f

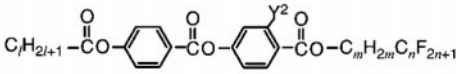

4g

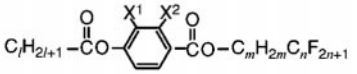

Compound no.	l	X_1	X_2	Y_1	Y_2	m	n	Phase sequences (°C)
4a-2A	9		F			3		cry (−12) SA (27) iso
4a-2B	10		F			4		cry (5) SA (22) iso
4a-2C	10		F			5		cry (0) SA (21) iso
4a-2D	9		F			6		cry (−7) SA (5) iso
4a-2E	9				F	7		cry (12) SC* (22) SA (26) iso
4a-2F	5			F		5		cry (1) SA (16) iso
4a-2G	7		F			5		cry (33) iso
4a-2H	9					6		cry (27) iso
4a-2I	10			F		8		cry (20) iso
4a-2J	10	F				8		cry (23) iso
4a-2K	10	F			F	8		cry (33) iso
4a-2L	10	F		F		8		cry (21) iso
4a-2M	10		F		F	8		cry (20) iso
4a-2N	10		F	F		8		cry (33) iso
4b-2P	9				F	3		cry (57) SA (77) iso
4b-2Q	9				F	5		cry (61) SA (72) iso
4b-2R	9				F	7		cry (66) SA (70) iso
4b-2S	9				F	8		cry (60) SA (70) iso
4b-2T	9				F	11		cry (40) SA (70) iso
4b-2U	9					7		cry (29) SA (69) iso
4a-2V	10				F	7		cry (16) SC* (23) ferri (26) SA (28) iso
4a-2W	9				F	$-C_5H_{10}OC_2H_5$		cry (30) anti (79) SC* (83) SA (92) iso
4c-2A	9	F				5		cry (25) iso
4c-2B	9	F				3		cry (37) iso
4c-2C	9	F				4		cry (5) SA (20) iso
4d-2A					F	6		cry (< −50) iso
4d-2B						6		cry (< −50) iso
4e-2A	9					1		cry (30) iso
4e-2B	9					3		cry (35) iso
4f-2A	9				F	1	1	cry (77) iso
4f-2B	9				F	1	2	cry (72) SA (81) iso
4g-2A	6					1	1	cry (31) iso
4g-2B	10					1	1	cry (28) iso
4g-2C	9		F			1	1	cry (30) iso
4g-2D	9	F				1	1	cry (34) iso
4g-2E	9					1	2	cry (28) iso
4g-2F	9					1	3	cry (27) iso
4g-2G	9					1	7	cry (57) iso
4g-2H	9					1	9	cry (79) iso
4g-2I	9					2	6	cry (60) iso
4g-2J	9		F			1	7	cry (51) iso
4g-2K	9	F				1	7	cry (45) iso
4-1A(3a-E16)								
4-1B(3a-E13)								
4-1C(3a-E1)								

Table 4 (*Continued*).

Mixture no.	Mixing ratios/mol	Phase sequences (°C)	E_s/V μm^{-1}	τ_{90}/μs	T/°C
4a-E1	4-1A:4a-2A = 80:20	cry < −20) ferri (75) SA (86) iso	2.6–2.0	88	30
4a-E2	4-1B:4a-2B = 80:20	cry (< −20) ferri (66) SA (77) iso	1.2–1.2	58	30
4a-E3	4-1B:4a-2C = 75:25	cry (< −20) ferri (62) SA (73) iso	1.4–1.4	77	30
4a-E4	4-1A:4a-2D = 80:20	cry (< −20) ferri (69) SA (75) iso	1.6–1.6	58	30
4a-E5	4-1B:4a-2E = 80:20	cry (< −20) ferri (67) SA (74) iso	1.4–1.4	65	30
4a-E6	4-1C:4a-2F = 80:20	cry (< −20) ferri (82) SA (92) iso	2.2–2.2	72	30
4a-E7	4-1C:4a-2G = 80:20	cry (< −20) ferri (79) SA (89) iso	2.0–2.0	65	30
4a-E8	4-1B:4a-2H = 80:20	cry (< −20) ferri (70) SA (78) iso	1.9–1.8	86	30
4a-E9	4-1B:4a-2I = 80:20	cry (< −20) ferri (62) SA (72) iso	1.2–1.2	69	30
4a-E10	4-1B:4a-2J = 80:20	cry (< −20) ferri (60) SA (70) iso	1.1–1.0	84	30
4a-E11	4-1C:4a-2K = 80:20	cry (< −20) ferri (71) SA (81) iso	1.3–1.3	68	30
4a-E12	4-1C:4a-2L = 80:20	cry (< −20) ferri (79) SA (83) iso	1.8–1.8	76	30
4a-E13	4-1C:4a-2M = 80:20	cry (< −20) ferri (74) SA (84) iso	2.0–2.0	70	30
4a-E14	4-1C:4a-2N = 80:20	cry (< −20) ferri (72) SA (85) iso	1.8–1.8	79	30
4a-E15	4-1B:4a-2A = 60:40	cry (< −20) ferri (51) SA (69) iso	1.5–1.2	79	30
4b-E16	4-1B:4b-2P = 75:25	cry (< −20) ferri (79) SA (98) iso	1.3–1.3	68	30
4b-E17	4-1B:4b-2Q = 75:25	cry (< −20) ferri (78) SA (92) iso	1.4–1.3	68	30
4b-E18	4-1B:4b-2R = 75:25	cry (< −20) ferri (81) SA (91) iso	1.3–1.3	65	30
4b-E19	4-1B:4b-2S = 75:25	cry (< −20) ferri (76) SA (87) iso	1.2–1.1	63	30
4b-E20	4-1B:4b-2T = 75:25	cry (< −20) ferri (74) SA (85) iso	1.0–1.0	59	30
4b-E21	4-1B:4b-2U = 75:25	cry (< −20) ferri (84) SA (93) iso	1.1–1.1	65	30
4b-E22	4-1B:4b-2P = 85:15	cry (< −20) ferri (83) SA (95) iso	1.3–1.3	64	30
4b-E23	4-1B:4b-2V = 70:30	cry (< −20) ferri (73) SA (82) iso	2.0–2.0	73	30
4b-CE1	4-1A:4b-2W = 80:20	cry (< −20) ferri (86) SA (93) iso	2.0–1.8	133	30
4c-E1	4-1A:4c-2A = 70:30	cry (< −10) ferri (68) SA (87) iso	1.3–1.2	64	30
4c-E2	4-1A:4c-2A = 60:40	cry (< −10) ferri (55) SA (82) iso	1.2–1.1	41	30
4c-E3	4-1A:4c-2B = 60:40	cry (< −10) ferri (52) SA (86) iso	1.2–1.2	50	30
4c-E4	4-1A:4c-2C = 60:40	cry (< −10) ferri (54) SA (79) iso	1.3–1.1	45	30
4d-E1	4-1A:4d-2A = 85:15	cry (< −20) ferri (77) SA (86) iso	1.2	203	30
4-1A			2.0–2.0	118	30
4-1B			1.5–1.4	88	30
4-1C			2.2–2.2	100	30
			$Tr(V=0)$ (%)		T/°C
4d-E1	4-1A:4d-2A = 80:20	cry (< −20) ferri (71) SA (82) iso	1.0		25
4e-E1	4-1A:4e-2A = 80:20	cry (< −20) ferri (91) SA (100) iso	2.0		25
4f-E1	4-1A:4f-2B = 80:20	cry (< −20) ferri (71) SA (83) iso	1.0		25
1A		cry (34) ferri (101) SA (103) iso	3.0		40

Table 5 Specifications of the materials developed by Mitsubishi Gas Chemical Company, Inc. The measurements were made using a homogeneous cell of about 2 μm thickness

	Materials specifications
Operating temperature	0–60 °C
Saturation voltage	4 V
Response speed	
Rise time	130 μs (5 V)
Fall time	230 μs (5 V)
Spontaneous polarization	1 mC m^{-2} (100 nC cm^{-2})
Tilt angle	28°

listed the highest temperatures, T_{max}(anti) and T_{max}(ferro), at which the antiferroelectric and ferroelectric phases remain in existence. Anyway, they confirmed the V-shaped switching in the homogeneous cells of the 36 mixtures (E1–E36) given in Table 2. Except for the mixtures, E7, E9, and E12 together with CE1, the antiferroelectric phase seems to emerge rather stably in free-standing films.

Table 3 summarizes compounds developed by Mitsubishi Gas Chemical Company, Inc. They also reported mixtures shown in Table 4. Their basic idea is to obtain materials which exhibit a single ferrielectric phase in a temperature range as wide as 100 °C or more. A compound of the general chemical formula **3a** with X = H or F and Y = H or F is the prototype that shows V-shaped switching as a single pure compound.[16,130] The phase identification was made in homeotropic cells and/or free-standing films, and V-shaped switching was observed in homogeneous cells when a ferrielectric phase emerges in free-standing films. As is seen in Table 3a, 44 examples (E1–E44) are listed together with 14 comparative examples (CE1–CE15). Some of them (E5, E6 and E41) have the ferrielectric phase in a temperature range as wide as 100 °C or more. As explained in Subsection 3.5, we suspect an almost continuous emergence of a variety of commensurate and/or incommensurate phase structures. It is a future problem to clarify the ferrielectric phase. Some compounds with the general chemical formulas **3b**, **3c**, **3d** and **3e** are listed in Tables 3b, 3c, 3d and 3e.[131–134] Three examples, E1–E3, in Table 3b are interesting compounds. They have a heavy element, chlorine, in the phenyl ring and show the apparently single ferrielectric phase. Consequently, we may be able to clarify a possible almost continuous emergence of a variety of commensurate and/or incommensurate phase structures by resonant X-ray scattering.[4] Table 4 summarizes mixtures developed by Mitsubishi Gas Chemical Company, Inc.[135–140] They tried to improve the V-shaped switching characteristics by mixing one of the compounds given in Table 3a that shows the ferrielectric phase with a phenyl ester compound that may or may not show a liquid crystalline mesophase. In this way, they recently announced the specifications of their materials as given in Table 5.

AM-LCDs using FRustoelectricity (FR-AM-LCDs) have already been prototyped. Saishu *et al.*[19] in Toshiba and Yoshida *et al.*[20] in Casio reported small FR-AM-LCDs in 1996 and 1997, respectively. Casio exhibited the prototype LCD in the 1997 Electronics Show, pictures and specifications of which are shown in Fig. 34. Since it is a QVGA display, the number of scanning lines is as small as 240. We can use 16.7 ms/240 lines = 69.6 μs for writing each line, where 16.7 ms is a frame period. The response speed of some existing FR-LC materials allows all dots on the line to attain the specified gray levels within the writing (charging) time. The small size,

low resolution FR-AM-LCD appears to be near commercialization.

A larger size, higher resolution prototype FR-AM-LCD was exhibited at Toshiba 'Tomorrow 21' in Tokyo, pictures and specifications of which are reproduced in Fig. 35. In the XGA display, the writing time is only 16.7 ms/768 lines = 21.7 μs. No existing frustoelectric materials have a fast enough response speed so that the specified gray levels can be attained within this short writing time. If the spontaneous polarization of the materials is negligibly small, as in any nematic materials, the holding voltage stays almost constant during the frame period. This ensures the attainment of the specified gray levels within response times as fast as 100 μs or so. Actually, however, the molecules continue to rotate because of inertia, and additional large spontaneous polarization emerges after entering into the holding (gate-off) time; the resulting depolarization field decreases the holding voltage seriously and hence the contrast ratio becomes markedly low. Since the polarity of an applied field inverts at every frame in ordinary ac driving, no accumulation is expected to increase the holding voltage and contrast ratio. Hasegawa *et al.*[141] and Okumura *et al.*[142] invented a quasi-dc driving method to overcome this difficulty. The polarity of the voltage applied to liquid crystals inverts at certain intervals of more than two frames. Thus, the holding voltage is kept increasing up to the value of the applied voltage. The transmittance attains the same value as that of the static driving so that a high contrast ratio can be provided. In this method, however, we cannot use a response speed as fast as *ca.* 100 μs fully. Some breakthrough in driving methods and/or materials appears to be necessary for the commercialization of FR-AM-LCD monitors.

It is important but takes time to develop FR-LC materials with faster response and smaller spontaneous polarization. Since both spontaneous polarization and antiferroelectric interaction result from the same transverse dipole moments of constituent molecules, the V-shaped switching needs some large spontaneous polarization. We could not fortell to what extent the spontaneous polarization is reduced, but 0.1 mC m^{-2} (10 nC m^{-2}) may be the smallest, which is about one order of magnitude reduction from the presently available value. Using large storage capacitance is also effective in decreasing the depolarization field, although this may reduce the TFT aperture ratio and hence the backlight transmittance efficiency. A higher driving voltage surely attains a faster response time, but inevitably results in a higher production cost. The above discussions presupposed line-by-line writing. The writing (charging) time decreases with increasing the number of pixels. Using a silicon chip instead of TFT makes us write a frame at the same time.[143,144] In frame-by-frame writing, the currently available response time, *ca.* 100 μs, is sufficiently fast. A field-sequential LCD, full-color video rate, will be realized without using a color filter. It is inevitably reflection type, and the cell gap must be less than 1 μm. In this way, FR-AM-LCD projectors are also promising for large size, high resolution displaying.

Acknowledgements

This work was partially supported by a Grant-in-Aid for COE Research (10CE2003) through the Monbusho in Japan.

References

1 A. D. L. Chandani, E. Gorecka, Y. Ouchi, H. Takezoe and A. Fukuda, *Jpn. J. Appl. Phys.*, 1989, **28**, L1265.
2 M. A. Osipov, in *Handbook of Liquid Crystals*, ed. D. Demus, J. Goodby, G. W. Gray, H.-W. Spiess and V. Vill, Wiley-VCH, Weinheim, 1998, Vol. 1, p. 40.
3 R. Schaetzing and J. D. Litster, in *Advances in Liquid Crystals*, ed. G. H. Brown, Academic Press, New York, 1983, vol. 4, p. 147.
4 P. Mach, R. Pindak, A.-M. Levelut, P. Barois, H. T. Nguyen, C. C. Huang and L. Furenlid, *Phys. Rev. Lett.*, 1998, **81**, 1015.
5 E. Gorecka, D. Pociecha, M. Glogarova and J. Mieczkowski, *Phys. Rev. Lett.*, 1998, **81**, 2946.
6 T. Isozaki, T. Fujikawa, H. Takezoe, A. Fukuda, T. Hagiwara, Y. Suzuki and I. Kawamura, *Jpn. J. Appl. Phys.*, 1992, **31**, L1435.
7 A. Fukuda, *Proc. Asia Display'95* (*Hamamatsu*), 1995, p. 61.
8 S. Inui, N. Iimura, T. Suzuki, H. Iwane, K. Miyachi, Y. Takanishi and A. Fukuda, *J. Mater. Chem.*, 1996, **6**, 671.
9 C. Tanaka, T. Fujiyama, T. Maruyama and S. Nishiyama, *Abstr. 21st Jpn. Liq. Cryst. Conf.*, 1995, p. 250.
10 J. Prost and R. Bruinsma, *Ferroelectrics*, 1993, **148**, 25.
11 M. A. Osipov and A. Fukuda, in preparation.
12 M. Yamashita and S. Miyazima, *Ferroelectrics*, 1993, **148**, 1.
13 H. Orihara and Y. Ishibasi, *Jpn. J. Appl. Phys.*, 1990, **29**, L115.
14 B. Zeks, R. Blinc and M. Cepic, *Ferroelectrics*, 1991, **122**, 221.
15 A. D. L. Chandani, T. Hagiwara, Y. Suzuki, Y. Ouchi, H. Takezoe and A. Fukuda, *Jpn. J. Appl. Phys.*, 1988, **27**, L729.
16 Y. Motoyama, T. Yui, M. Johno and M. Itoh, *Jpn. Pat. Gaz.*, 1996, H8–337 555.
17 S. S. Seomun, Y. Takanishi, K. Ishikawa, H. Takezoe and A. Fukuda, *Jpn. J. Appl. Phys.*, 1997, **36**, 3586.
18 A. Fukuda and T. Matsumoto, *Proc. IDW'97 (Nagoya)*, 1997, p. 355.
19 T. Saishu, K. Takatoh, R. Iida, H. Nagata and Y. Mori, *SID 96 Digest*, 1996, 703.
20 T. Yoshida, T. Tanaka, J. Ogura, H. Wakai and H. Aoki, *SID 97 Digest*, 1997, 841.
21 A. Fukuda, Y. Takanishi, T. Isozaki, K. Ishikawa and H. Takezoe, *J. Mater. Chem.*, 1994, **4**, 997.
22 I. Nishiyama, *Adv. Mater.*, 1994, **6**, 996.
23 Y. Ouchi, Y. Yoshioka, H. Ishii, K. Seki, M. Kitamura, R. Noyori, Y. Takanishi and I. Nishiyama, *J. Mater. Chem.*, 1995, **5**, 2297.
24 B. Jin, Z. Ling, Y. Takanishi, K. Ishikawa, H. Takezoe, A. Fukuda, M. Kakimoto and T. Kitazume, *Phys. Rev. E*, 1996, **53**, R4295.
25 H. Yin, B. Jin, Y. Takanishi, K. Ishikawa, H. Takezoe and A. Fukuda, *Mol. Cryst. Liq. Cryst.*, 1997, **303**, 285.
26 T. Nakai, S. Miyajima, Y. Takanishi, S. Yoshida and A. Fukuda, *J. Phys. Chem. B*, 1999, **103**, 406.
27 S. Yoshida, B. Jin, Y. Takanishi, K. Tokumaru, K. Ishikawa, H. Takezoe, A. Fukuda, T. Kusumoto, T. Nakai and S. Miyajima, *J. Phys. Soc. Jpn.*, 1999, **68**, 9.
28 K. Mikami, T. Yajima, M. Terada, S. Kawauchi, Y. Suzuki and I. Kobayashi, *Chem. Lett.*, 1996, 861.
29 I. Kobayashi, Y. Suzuki, T. Yajima, S. Kawauchi, M. Terada and K. Mikami, *Mol. Cryst. Liq. Cryst.*, 1997, **303**, 165.
30 K. Okuyama, N. Kawano, S. Uehori, K. Noguchi, N. Okabe, Y. Suzuki and I. Kawamura, *Mol. Cryst. Liq. Cryst.*, 1996, **276**, 193.
31 K. Miyachi, J. Matsushima, Y. Takanishi, K. Ishikwa, H. Takezoe and A. Fukuda, *Phys. Rev. E*, 1995, **52**, R2153.
32 K. H. Kim, K. Ishikawa, H. Takezoe and A. Fukuda, *Phys. Rev. E*, 1995, **51**, 2166.
33 D. R. Link, J. E. Maclennan and N. A. Clark, *Phys. Rev. Lett.*, 1996, **77**, 2237.
34 S.-D. Lee and J.-H. Lee, *Proc. IDW'97* (Nagoya), 1997, p. 69.
35 A. Fukuda, S. S. Seomun, T. Takahashi, Y. Takanishi and K. Ishikawa, *Mol. Cryst. Liq. Cryst.*, 1997, **303**, 379.
36 I. Nishiyama and J. W. Goodby, *J. Mater. Chem.*, 1992, **2**, 1015.
37 Y. Takanishi, K. Hiraoka, V. K. Agrawal, H. Takezoe, A. Fukuda and M. Matsushita, *Jpn. J. Appl. Phys.*, 1991, **30**, 2023.
38 A. D. L. Chandani, Y. Ouchi, H. Takezoe, A. Fukuda, K. Terashima, K. Furukawa and A. Kishi, *Jpn. J. Appl. Phys.*, 1989, **28**, L1261.
39 A. Jakli, T. Scharf and A. Saupe, *J. Appl. Phys.*, 1999, **85**, 1101.
40 A. Jakli, T. Scharf and A. Saupe, *Proc. Freiburge Arbeitstagung*, (Freiburg), ed. G. Bauer, 1995, p. 12.
41 H. Uehara, Y. Iino and J. Hatano, *Jpn. J. Appl. Phys.*, 1997, **36**, 6118.
42 T. Sako, Y. Kimura, R. Hayakawa, N. Okabe and Y. Suzuki, *Jpn. J. Appl. Phys.*, 1996, **35**, L114.
43 H. F. Gleeson, J. T. Mills, L. Baylis, J. W. Goodby, A. Seed, M. Hird and P. Styring, *17th Int. Liq. Cryst. Conf. (Strasbourg)*, 1998, P2–187, p. P-133.
44 E. Gorecka, A. D. L. Chandani, Y. Ouchi, H. Takezoe and A. Fukuda, *Jpn. J. Appl. Phys.*, 1990, **29**, 131.
45 N. Okabe, Y. Suzuki, I. Kawamura, T. Isozaki, H. Takezoe and A. Fukuda, *Jpn. J. Appl. Phys.*, 1992, **31**, L793.

46 T. Isozaki, T. Fujikawa, H. Takezoe, A. Fukuda, T. Hagiwara, Y. Suzuki and I. Kawamura, *Phys. Rev. B*, 1993, **48**, 13 439.
47 T. Isozaki, H. Takezoe, A. Fukuda, Y. Suzuki and I. Kawamura, *J. Mater. Chem*., 1994, **4**, 237.
48 J. Hatano, Y. Hanakai, H. Furue, H. Uehara, S. Saito and K. Murashiro, *Jpn. J. Appl. Phys*., 1994, **33**, 5498.
49 Yu. P. Panarin, O. Kalinovskaya, J. K. Vij and J. W. Goodby, *Phys. Rev. E,* 1997, **55**, 4345.
50 K. Itoh, M. Kabe, K. Miyachi, Y. Takanishi, K. Ishikawa, H. Takezoe and A. Fukuda, *J. Mater. Chem*., 1997, **7**, 407.
51 K. Yamada, Y. Takanishi, K. Ishikawa, H. Takezoe, A. Fukuda and M. A. Osipov, *Phys. Rev. E*, 1997, **56**, R43.
52 M. Neundorf, Y. Takanishi, A. Fukuda, S. Saito, K. Murashiro, T. Inukai and D. Demus, *J. Mater. Chem*., 1995, **5**, 2221.
53 P. G. de Gennes and J. Prost, *The Physics of Liquid Crystals*, 2nd Edn., Clarendon Press, Oxford, 1993, p. 547.
54 G. Heppke, P. Kleineberg and D. Lötzsch, *Liq. Cryst.*, 1993, **14**, 67.
55 H. T. Nguyen, J. C. Couillon, P. Cluzeau, G. Sigaud, C. Destrade and N. Isaert, *Liq. Cryst*., 1994, **17**, 571.
56 K. Ema, H. Yao, I. Kawamura, T. Chan and C. W. Garland, *Phys. Rev. E*, 1993, **47**, 1203.
57 S. Asahina, M. Sorai, A. Fukuda, H. Takezoe, K. Furukawa, K. Terashima, Y. Suzuki and I. Kawamura, *Liq. Cryst*., 1997, **23**, 339.
58 K. Ema, J. Watanabe, A. Takagi and H. Yao, *Phys. Rev. E*, 1995, **52**, 1216.
59 T. Aoki, Ke Chao, A. Fukuda, Y. Takanishi, K. Ishikawa, H. Takezoe and H. T. Nguyen, *Abstr. 25th Jpn. Liq. Cryst. Conf.*, 1999, in the press.
60 B. Jaffe, W. R. Cook, Jr. and H. Jaffe, *Piezoelectric Ceramics*, Academic Press (London and New York), 1971, p. 14.
61 K. Hiraoka, Y. Takanishi, K. Skarp, H. Takezoe and A. Fukuda, *Jpn. J. Appl. Phys*., 1991, **30**, L1891.
62 H. Takezoe, J. Lee, Y. Ouchi and A. Fukuda, *Mol. Cryst. Liq. Cryst*., 1991, **202**, 85.
63 P. Bak and R. Bruinsma, *Phys. Rev. Lett*., 1982, **49**, 249.
64 R. Bruinsma and P. Bak, *Phys. Rev. B*, 1983, **27**, 5824.
65 M. E. Fisher and W. Selke, *Phys. Rev. Lett*., 1980, **44**, 1502.
66 P. Bak and J. von Boehm, *Phys. Rev. B*, 1980, **21**, 5297.
67 A. Roy and N. V. Madhusudana, *Europhys. Lett*., 1996, **36**, 221.
68 M. Cepic and B. Zeks, *Mol. Cryst. Liq. Cryst.*, 1995, **263**, 61.
69 A. Roy and N. V. Madhusudana, *Europhys. Lett.*, 1998, **41**, 501.
70 K. Miyachi, M. Kabe, K. Ishikawa, H. Takezoe and A. Fukuda, *Ferroelectrics*, 1993, **147**, 147.
71 M. Glogavova, H. Sverenyak, A. Fukuda and H. Takezoe, *Liq. Cryst*., 1993, **14**, 463.
72 M. Cepic, G. Heppke, J.-M. Hollidt, D. Lötzsch and B. Zeks, *Ferroelectrics*, 1993, **147**, 1159.
73 S. S. Seomun, T. Gouda, Y. Takanishi, K. Ishikawa, H. Takezoe and A. Fukuda, *Liq. Cryst*., 1999, **26**, 151.
74 (*a*) A. D. L. Chandani, Y. Cui, S. S. Seomun, Y. Takanishi, K. Ishikawa, H. Takezoe and A. Fukuda, *Liq. Cryst*., 1999, **26**, 167; (*b*) K. Hiraoka, T. Matsumoto, A. Fukuda and Y. Takarishi, unpublished results.
75 K. Ema, H. Yao, T. Matsumoto, A. Fukuda, Y. Takanishi and H. Takezoe, *Abstr. 24th Jpn. Liq. Cryst. Conf.*, 1998, p. 268.
76 H. Sun, H. Orihara and Y. Ishibashi, *J. Phys. Soc. Jpn.*, 1991, **60**, 4175.
77 H. Sun, H. Orihara and Y. Ishibashi, *J. Phys. Soc. Jpn.*, 1993, **62**, 2706.
78 B. Zeks and M. Cepic, *Liq. Cryst.*, 1993, **14**, 445.
79 V. L. Lorman, A. A. Bulbitch and P. Toredano, *Phys. Rev. E*, 1994, **49**, 1367.
80 V. L. Lorman, *Mol. Cryst. Liq. Cryst*., 1995, **262**, 437.
81 S. A. Pikin, S. Hiller and W. Haase, *Mol. Cryst. Liq. Cryst.*, 1995, **262**, 425.
82 M. Yamashita, *Ferroelectrics*, 1996, **181**, 201.
83 M. Yamashita, *Mol. Cryst. Liq. Cryst*., 1997, **303**, 153.
84 M. Yamashita and S. Tanaka, *Jpn. J. Appl. Phys*., 1998, **37**, L528.
85 S. Tanaka and M. Yamashita, *Jpn. J. Appl. Phys*., 1999, **38**, L139.
86 M. Nakagawa, *J. Phys. Soc. Jpn*., 1993, **62**, 2260.
87 T. Koda and H. Kimura, *Ferroelectrics*, 1993, **148**, 31.
88 T. Koda and H. Kimura, *J. Phys. Soc. Jpn*., 1995, **64**, 3787.
89 T. Koda and H. Kimura, *J. Phys. Soc. Jpn*., 1996, **65**, 2880.
90 Y. Yamada and N. Hamaya, *J. Phys. Soc. Jpn*., 1983, **52**, 3466.
91 M. Skarabot, M. Cepic, B. Zeks, R. Blinc, G. Heppke, A. V. Kityk and I. Musevic, *Phys. Rev. E*, 1998, **58**, 575.
92 B. Zeks and M. Cepic, *Proc. SPIE*, 1998, **3318**, 68.
93 X. Y. Wang and P. L. Taylor, *Phys. Rev. Lett*., 1996, **76**, 640.
94 E. Gorecka, M. Glogarova, H. Sverenyak and L. Lejcek, *Ferroelectrics*, 1996, **178**, 101.
95 G. A. Hinshaw, Jr., R. G. Petschek and R. A. Pelovits, *Phys. Rev. Lett*., 1988, **60**, 1864.
96 E. Demikhov and H. Stegemeyer, *Liq. Cryst.*, 1995, **18**, 37.
97 M. Yamashita, *J. Phys. Soc. Jpn*., 1996, **65**, 2122.
98 M. Yamashita, *J. Phys. Soc. Jpn*., 1996, **65**, 2904.
99 M. Yamashita, *J. Phys. Soc. Jpn*., 1997, **66**, 130.
100 M. Yamashita, *Kotaibuturi* (in Japanese), 1996, **31**, 1005.
101 M. Yamashita, *J. Phys. Soc. Jpn*., 1998, **67**, 198.
102 M. Yamashita and S. Takeno, *J. Phys. Soc. Jpn*., 1999, **68**, 1473.
103 M. Yamashita and S. Tanaka, *J. Phys. Soc. Jpn*., 1999, **68**, 1797.
104 M. Yamashita and H. Nakano, *Prog. Theor. Phys*., 1976, **56**, 1042.
105 M. Yamashita and H. Nakano, *Prog. Theor. Phys*., 1977, **57**, 759.
106 For example, Th. Niemeijer and J. M. J. van Leeuwen, *Phase Transitions and Critical Phenomena*, ed. C. Domb and M. Green, Academic Press, London, 1976, Vol. 6, Ch. 7.
107 K. Miyachi and A. Fukuda, in *Handbook of Liquid Crystals*, ed. D. Demus, J. Goodby, G. W. Gray, H.-W. Spiess and V. Vill, Wiley-VCH, Weinheim, 1998, Vol. 2B, p. 665.
108 T. Matsumoto and A. Fukuda, *Liq. Cryst. Today*, 1998, **8**(6), 4.
109 A. Fukuda, *Abstr. 17th Int. Liq. Cryst. Conf.* (*Strasbourg*), 1998, Plenary B, p. O-11.
110 S. S. Seomun, Thesis (Doctor of Engineering), Tokyo Institute of Technology, 1998.
111 (*a*) P. Rudquist, J. P. F. Lagerwall, M. Buivydas, F. Gouda, S. T. Lagerwall, R. F. Shao, D. Coleman, S. Bardon, D. R. Link, T. Bellini, J. E. Maclennan, S. H. Chen, D. M. Walba, N. A. Clark and X.-H. Chen, *SID 99 Digest*, 1999, 409; (*b*) P. Rudquist, J. P. F. Lagerwall, M. Buivydas, F. Gouda, S. T. Lagerwall, N. A. Clark, J. E. Maclennan, R. Shao, D. A. Coleman, S. Bardon, T. Bellini, D. R. Link, G. Natale, M. A. Glaser, D. M. Walba, M. D. Wand and X.-H. Chen, *J. Mater. Chem.*, 1999, **9**, 1257.
112 S. S. Seomun, Y. Takanishi, K. Ishikawa, H. Takezoe, A. Fukuda, C. Tanaka, T. Fujiyama, T. Maruyama and S. Nishiyama, *Mol. Cryst. Liq. Cryst*., 1997, **303**, 181.
113 S. S. Seomun, T. Gouda, T. Takanishi, K. Ishikawa, H. Takezoe, A. Fukuda, C. Tanaka, T. Fujiyama, T. Maruyama and S. Nishiyama, *Proc. IDW '96* (*Kobe*), 1996, p. 61.
114 H. Pauwels, B. Verweire and K. D'have, *Abstr. 17th Int. Liq. Cryst. Conf.* (*Strasbourg*), 1998, P4–64, p. P-232.
115 H. Pauwels, B. Verweire, K. D'have and J. Fornier, *SID 98 Digest*, 1998, 1175.
116 H. Takezoe, A. D. L. Chandani, S. S. Seomun, B. Park, D. S. Hermann, Y. Takanishi and K. Ishikawa, *Proc. Asia Display 98 (Seoul)*, p. 23.
117 B. Park, S. S. Seomun, M. Nakata, M. Takahashi, Y. Takanishi, K. Ishikawa, and H. Takezoe, *Jpn. J. Appl. Phys.*, 1999, in the press.
118 K. Ishikawa, Y. Ouchi, T. Uemura, T. Tsuchiya, H. Takezoe and A. Fukuda, *Mol. Cryst. Liq. Cryst*., 1985, **122**, 175.
119 Y. Suzuki, T. Hagiwara, I. Kawamura, N. Okamura, T. Kitazume, M. Kakimoto, Y. Imai, Y. Ouchi, H. Takezoe and A. Fukuda, *Liq. Cryst*., 1989, **6**, 167.
120 M. Johno, K. Itoh, J. Lee, Y. Ouchi, H. Takezoe, A. Fukuda and T. Kitazume, *Jpn. J. Appl. Phys*., 1990, **29**, L107.
121 J.-F. Li, X.-Y. Wang, E. Kangas, P. L. Taylor, C. Rosenblatt, Y. Suzuki and P. E. Cladis, *Phys. Rev. B*, 1995, **52**, R13075.
122 J. Fünfschilling and M. Schadt, *J. Appl. Phys*., 1989, **66**, 3877.
123 S. S. Seomun, B. Park, A. D. L. Chandani, D. S. Hermann, Y. Takanishi, K. Ishikawa, H. Takezoe and A. Fukuda, *Jpn. J. Appl. Phys*., 1998, **37**, L691.
124 M. Ohta, M. Oh-e and K. Kondo, *Proc. Asia Display '95 (Hamamatsu)*, 1995, p. 577.
125 J. Mukai, H. Mazaki, Y. Satoh, Y. Kobori, T. Kaminaka, T. Toyooka and H. Itoh, *Proc. Asia Display '95 (Hamamatsu)*, 1995, p. 949.
126 H. Mori, Y. Itoh, Y. Nishimura, T. Nakamura and Y. Shinagawa, *Proc. AM-LCD '96/IDW '96 (Kobe)*, 1996, Vol. 1, p. 189.
127 Y. Koike, S. Kataoka, T. Sasaki, H. Chida, H. Tsuda, A. Takeda, K. Ohmuro, T. Sasabayashi and K. Okamoto, *Proc. IDW '97 (Nagoya)*, 1997, p. 159.
128 G.-P. Chen, M. Yamaguti, N. Ito, T. Aoki and A. Fukuda, *Jpn. J. Appl. Phys*., 1999, **38**, L646.
129 S. Nishiyama, Y. Tatsuki, T. Fujiyama and Ch. Tanaka, *Jpn. Pat. Gaz.*, 1997, H9–48 970.
130 H. Mineta, T. Yui, M. Johno and T. Toyama, *Jpn. Pat. Gaz.*, 1997, H9–302 342.
131 H. Mineta, Y. Motoyama, T. Yui and M. Johno, *Jpn. Pat. Gaz.*, H10–45 673.

132 H. Mineta, T. Yui, M. Johno and T. Matsuomo, *Jpn. Pat. Gaz.*, 1998, H10–67 715.
133 T. Mine, M. Johno, T. Yui and T. Matsumoto, *Jpn. Pat. Gaz.*, 1998, H10–316 626.
134 Y. Motoyma, M. Johno, T. Yui and T. Matsumoto, *Jpn. Pat. Gaz.*, 1998, H10–324 666.
135 M. Johno, T. Matsumoto, T. Yui and M. Itoh, *Jpn. Pat. Gaz.*, 1997, H9–40 960.
136 M. Johno, H. Mineta, T. Yui and Y. Motoyama, *Jpn. Pat. Gaz.*, 1998, H10–25 477.
137 M. Johno, T. Yui, H. Mineta and Y. Motoyama, *Jpn. Pat. Gaz.*, 1998, H10–120 629.
138 M. Johno, Y. Motoyama, T. Yui and T. Matsumoto, *Jpn. Pat. Gaz.*, 1998, H10–245 363.
139 Y. Motoyama, T. Yui, M. Johno and H. Mineta, *Jpn. Pat. Gaz.*, 1998, H10–245 364.
140 M. Johno, Y. Motoyama, T. Yui and T. Matsumoto, *Jpn. Pat. Gaz.*, 1998, H10–330 321.
141 R. Hasegawa, H. Fujiwara, H. Nagata, T. Saishu, R. Iida, Y. Hara, M. Akiyama, H. Okumura and K. Takatoh, *Proc. AM-LCD97*, 1997, p. 119.
142 H. Okumura, M. Akiyama, K. Takatoh and Y. Uematsu, *SID 98 Digest*, 1998, 1171.
143 M. Hosokawa, K. Oguchi, M. Ikeda, S. Yazawa and K. Endo, *SID 81 Digest*, 1981, 114.
144 P. Cacharelis, U. S. Kim, J. Frazee, P. Moore, K. Brown, R. Luttrell, P. Renteln and R. Flack, *SID 97 Digest*, 1997, 289.

Paper 9/03273H